JOURNAL OF GUIDANCE, CONTROL, AND DYNAMICS
Vol. 38, No. 9, September 2015

Multiple-Object Space Surveillance Tracking Using Finite-Set Statistics

Kyle J. DeMars*
Missouri University of Science and Technology, Rolla, Missouri 65409
Islam I. Hussein†
Applied Defense Solutions, Columbia, Maryland 21044
Carolin Frueh‡
Purdue University, West Lafayette, Indiana 47907
and
Moriba K. Jah§ and R. Scott Erwin¶
U.S. Air Force Research Laboratory, Kirtland Air Force Base, New Mexico 87117

DOI: 10.2514/1.G000987

The dynamic tracking of objects is, in general, concerned with state estimation using imperfect data. Multiple object tracking adds the difficulty of encountering unknown associations between the collected data and the objects. State estimation of objects necessitates the prediction of uncertainty through nonlinear (in the general case) dynamical systems and the processing of nonlinear (in the general case) measurement data in order to provide corrections that refine the system uncertainty, where the uncertainty may be non-Gaussian in nature. The sensors, which provide the measurement data, are imperfect with possible misdetections, false alarms, and noise-affected data. The resulting measurements are inherently unassociated upon reception. In this paper, a Bayesian method for tracking an arbitrary, but known, number of objects is developed. The method is based on finite-set statistics coupled with finite mixture model representations of the multiobject probability density function. Instead of relying on first-moment approximations, such as the probability hypothesis density filter, to the full multiobject Bayesian posterior, as is often done for multiobject filtering, the proposed method operates directly on the exact Bayesian posterior. Results are presented for application of the method to the problem of tracking multiple space objects using synthetic line-of-sight data.

I. Introduction

ABOUT 100,000 objects 1 cm in size or larger populate the space around Earth, which increases the need for new methods and techniques that can contribute to the core elements of space situational awareness (SSA): detection of new objects, tracking of detected objects, and characterization of tracked objects. These tasks need to be performed in the presence of noisy data, misdetections, and false alarms from clutter sources. Moreover, streams of data are unassociated with objects of interest and are not readily distinguished from clutter.

Whereas most SSA literature treats the core elements of detection [1], tracking [2], characterization [3], and data association (usually within a tracking context) [4–6] independently from each other, the research approach advocated in this work is to seek an integrated approach to all of these problems. In treating detection, tracking, characterization, and data association separately, valuable information can be lost. By taking into account the fact that detection, tracking, characterization, and data association are interdependent, information loss is limited. For example, object type may define some basic shape characteristics that affect motion (e.g., drag coefficient for a low-Earth-orbit object), and thus provides information about the object's dynamics and its track, and vice versa. Methods that explicitly account for these interdependencies are therefore at an advantage over methods that assume independence between the problems.

The technique proposed in this work for approaching the SSA problem is based on finite-set statistics (FISST) [7,8]. FISST provides a Bayesian framework for handling multiobject estimation problems that allows for the joint estimation of object state of existence, type, and tracking. Inherent to FISST is a solution to the data association problem. The greatest challenge in implementing FISST in real time, which is critical to any viable SSA solution, is computational burden. The first-order probability hypothesis density (PHD) approach has been proposed as a computationally tractable approach to applying FISST [8,9]. PHD can further employ a Gaussian mixture (GM) or a particle filter approximation to further reduce the computational burden (by removing the need to discretize the state space) at the expense of simplifying assumptions. In this paper, a GM approximation is developed and applied, not to the first-order PHD approximation but to the original predictor and corrector equations derived from FISST. This eliminates any information loss associated with using the first-order PHD approximation. The approach pursued here is similar in spirit to the concept of the "para-Gaussian" that was described in [8] and [10]. The para-Gaussian approach is founded upon modeling the conventional probability density functions (PDFs) as Gaussian mixtures and applying this model to formulate a multitarget multi-Bernoulli filter [8]. This differs from a Gaussian mixture application of the Gaussian mixture PHD filter or cardinalized PHD filter where the Gaussian mixture is applied to the first-moment representation of the multiobject density.

The particular GM technique used for the approximation is the adaptive entropy-based Gaussian-mixture information synthesis (AEGIS) method [11,12], which is an estimation approach for nonlinear continuous dynamical systems. AEGIS implements a GM model representation of the probability density function that is adapted online via splitting of the GM components whenever an

Presented as Paper 2012-4807 at the AIAA/AAS Astrodynamics Specialist Conference, Minneapolis, MN, 13–16 August 2012; received 17 August 2014; revision received 26 November 2014; accepted for publication 2 December 2014; published online 9 March 2015.

*Assistant Professor, Department of Mechanical and Aerospace Engineering.
†Aerospace Engineer.
‡Assistant Professor, School of Aeronautics and Astronautics.
§Senior Research Aerospace Engineer, Space Vehicles Directorate.
¶Principle Research Aerospace Engineer, Space Vehicles Directorate.

entropy-based detection of nonlinearity-induced distortions of the Gaussian components is triggered during the forward propagation of the PDF. In doing so, the GM approximation adaptively includes additional components as nonlinearity is encountered and can therefore be used to more accurately approximate the PDF.

In a recent paper, an AEGIS-based approximation to FISST was introduced and applied to joint detection and tracking of a simple single-object SSA scenario [13]. The present paper generalizes the application of AEGIS-FISST to the case where the number of objects is arbitrary (i.e., more than one) and is known (hence eliminating the detection problem). Sensor returns are assumed to be noisy with the possibility of misdetections and false alarms. As opposed to the simple Bernoulli model used in [13], false alarms are assumed to be generated from a Poisson clutter-generating distribution.

To summarize, the main contributions of this paper are 1) the use of the AEGIS approach to approximate the complete, unapproximated FISST predictor and corrector equations; and 2) the application of this approach to the problem of tracking of space objects in the presence of clutter, false alarm, and misdetections. The remainder of the paper is organized as follows. The theory behind FISST is briefly summarized in Sec. II. The AEGIS approach is briefly summarized in Sec. III. Section IV presents the full multiobject tracking filtering equations, which are then approximated using an AEGIS-based GM approach in Sec. V. A description of how to extract state estimates from the AEGIS-FISST multiobject distributions, and a discussion on scoring the distance etween multiobject true and estimated states is given in Sec. VI. Section VII provides a detailed description of the sensor model used in the simulations. Simulation results and an accompanying discussion of the results are presented in Sec. VIII. Finally, Sec. IX summarizes the findings of the paper.

II. Brief Introduction to FISST-Based Filtering

As opposed to purely discrete or purely continuous Bayesian inference, FISST makes use of set-valued random variables. For example, if W is taken to be the set of all possible space object types, then $x_d \in W$ is the discrete component of the state that describes a space object's type (and hence its dynamic model) and $\boldsymbol{x} \in \mathbb{R}^s$ is the continuous component of the state (e.g., the specification of the object's position and velocity), and then the set-valued random variable corresponding to the hybrid system state is $X = \{x_d, \boldsymbol{x}\}$. On the other hand, in a detection and tracking problem, the set-valued state is $X = (n, \boldsymbol{X})$, where n is the discrete component that describes the number of objects in the search space and

$$\boldsymbol{X} = [\boldsymbol{x}_1^T \boldsymbol{x}_2^T \ldots \boldsymbol{x}_n^T]^T \in \mathbb{R}^{sn}$$

describes the states of these objects, where the state of an object in this work is the collection of the position and velocity of the object. Notice here the explicit dependence of the dimension of the continuous state-space $\mathbb{R}^{sn}$ on the discrete component n of the state. For brevity, the set-valued state is written as $X = \{\boldsymbol{x}_1, \boldsymbol{x}_2, \ldots, \boldsymbol{x}_n\}$ in the detection and tracking problem. Similar definitions apply to the set-valued measurement variable $Z = \{\boldsymbol{z}_1, \boldsymbol{z}_2, \ldots, \boldsymbol{z}_m\}$ with m number of sensor returns and, where $\boldsymbol{z}_i \in \mathbb{R}^q$, $i = 1, \ldots, m$, is the value of each q-dimensional return.

Bayes' rule takes on exactly the same form in the hybrid FISST approach as it does in purely continuous and purely discrete problems; that is,

$$f_{k+1|k}(X|Z^{(k)}) = \int f_{k+1|k}(X|X') f_{k|k}(X'|Z^{(k)}) \delta X' \tag{1}$$

$$f_{k+1|k+1}(X|Z^{(k+1)}) = \frac{f_{k+1}(Z_{k+1}|X) f_{k+1|k}(X|Z^{(k)})}{f_{k+1}(Z_{k+1}|Z^{(k)})} \tag{2}$$

where

$$Z^{(k+1)} = \{Z_1, \ldots, Z_{k+1}\}$$

is the collection of the measurement sets up to and including time $k+1$, and where $f_{k+1|k}(X|X')$ is the multiobject Markov transitional density. The function $f_{k+1}(Z|X)$ is the multiobject likelihood function that describes the likelihood of getting a measurement Z_{k+1} given the state X. Equation (1) is the prediction step, and Eq. (2) is the update or corrector step. The normalization factor in the update step is called the Bayes factor, which is given by

$$f_{k+1}(Z_{k+1}|Z^{(k)}) = \int f_{k+1}(Z_{k+1}|X) f_{k+1|k}(X|Z^{(k)}) \delta X \tag{3}$$

Notice that the integrals that appear in Eqs. (1) and (3) are set integrals, denoted by the variable of integration δX as opposed to $\mathrm{d}X$ for a standard integral. For multiobject tracking, the set integral of a scalar-valued set function $g(X)$ is defined to be the standard integral of g over the continuous component, summed over all possible discrete values. This gives the set integral to be [7,8]

$$\int g(X)\delta X = g(X = \varnothing) + \sum_{i=1}^{\infty} \frac{1}{i!} \int g(\{\boldsymbol{x}_1, \ldots, \boldsymbol{x}_i\})\, \mathrm{d}\boldsymbol{x}_1 \cdots \mathrm{d}\boldsymbol{x}_i \tag{4}$$

where the factorial coefficient accounts for all of the possible orderings of X as evaluated in the function g and the summation over i are the aforementioned summation over all possible discrete values, i.e., all possible cardinalities of the set X.

III. Brief Introduction to AEGIS

Standard implementations of Gaussian mixture propagation algorithms assume that the component weights remain constant over the duration of the propagation span and so do not incorporate a method for online refinement of the Gaussian mixture (see, for example, [14] and [15]). Some methods, such as the adaptive Gaussian mixture approach, provide a means for adaptive weight variation without a mechanism to vary (coarsen or refine) the number of Gaussian components [16]. The AEGIS method approaches the problem of adapting the weights of the GM PDF by monitoring nonlinearity-induced distortions of the Gaussian components during the propagation of the PDF and using a splitting algorithm to increase the accuracy of linearization, thereby allowing the filter to modify the GM components (weight value and cardinality) in such a way so as to avoid linearization errors.

A. AEGIS Method

Consider the nonlinear dynamical system governed by the differential equation

$$\dot{\boldsymbol{x}}(t) = \boldsymbol{f}(\boldsymbol{x}(t)), \qquad \boldsymbol{x}(t_0) = \boldsymbol{x}_0$$

where $\boldsymbol{x}(t)$ is the non-set-valued continuous state of the system, $\boldsymbol{f}(\cdot)$ represents the sufficiently differentiable nonlinear dynamics of the system, and $\boldsymbol{x}_0$ is the initial condition. The initial condition is assumed to be random with PDF $f_{0|0}(\boldsymbol{x})$.

1. Detecting Nonlinearity-Induced Distortions to the GM During Propagation

An integral aspect of the AEGIS propagation scheme is the detection of nonlinearity during the propagation of uncertainty. The method employed in the AEGIS approach is based on a property derived from the differential entropy for linearized dynamical systems that allows for the detection of nonlinearity without employing linearization-based methods. It can be shown that the differential entropy for a linearized, Gaussian system evolves as [17,18]

$$\dot{H}(\boldsymbol{x}) = \mathrm{trace}\{\boldsymbol{F}(\boldsymbol{m}(t))\} \tag{5}$$

where $\boldsymbol{F}(\boldsymbol{m}(t))$ is the dynamics Jacobian matrix, and $\boldsymbol{m}(t)$ is the time-varying mean of the Gaussian distribution. The value of the entropy for a linearized system can be determined by numerically integrating Eq. (5) with an appropriate initial condition, which requires only the evaluation of the trace of the linearized dynamics Jacobian. In parallel, a nonlinear implementation of the integration of the covariance matrix (e.g., the unscented Kalman filter (UKF) [19]) is considered, which allows a nonlinear determination of the differential entropy. Any deviation between these values of entropy therefore serves as an indication that nonlinearity is impacting the solution. When the difference between the linearized-predicted entropy and the nonlinear computation of the entropy exceeds a user-defined threshold, nonlinearity has been detected in the propagation of the uncertainty, the propagation is halted, a splitting algorithm is applied to the Gaussian distribution, and propagation resumes with the adapted distribution.

2. Propagation

Consider the time propagation of the PDF and consider the time interval $t \in [t_k, t_{k+1}]$. It is desired to approximate the conditional PDF at time t_k via

$$f_{k|k}(\boldsymbol{x}|Z^{(k)}) = \sum_{i=1}^{\bar{N}} \bar{w}_i p_g(\boldsymbol{x}; \bar{\boldsymbol{\mu}}_i, \bar{\boldsymbol{P}}_i) \tag{6}$$

where $p_g(\boldsymbol{x}; \bar{\boldsymbol{\mu}}_i, \bar{\boldsymbol{P}}_i)$ is a Gaussian distribution in $\boldsymbol{x}$ with mean $\bar{\boldsymbol{\mu}}_i$ and covariance $\bar{\boldsymbol{P}}_i$, and where $\bar{w}_i$ is the weight of the ith GM component ($i = 1 \ldots, \bar{N}$) with

$$\sum_{i=1}^{\bar{N}} \bar{w}_i = 1$$

The propagated PDF is then given by

$$f_{k+1|k}(\boldsymbol{x}|Z^{(k)}) = \sum_{i=1}^{\tilde{N}} \tilde{w}_i p_g(\boldsymbol{x}; \tilde{\boldsymbol{\mu}}_i, \tilde{\boldsymbol{P}}_i) \tag{7}$$

where $\tilde{w}_i$, $\tilde{\boldsymbol{\mu}}_i$, and $\tilde{\boldsymbol{P}}_i$, $i = 1, \ldots, \tilde{N}$, are the weight, mean, and covariance of the ith propagated GM component. It should be noted that, due to the splitting algorithm described previously, the number of components in $f_{k+1|k}(\boldsymbol{x}|Z^{(k)})$, given by $\tilde{N}$, may now be different from the number of components in $f_{k|k}(\boldsymbol{x}|Z^{(k)})$, given by $\bar{N}$.

To propagate the PDF forward in time, a nonlinear algorithm such as the UKF is applied to each component of the GM PDF. Simultaneously, the linearized differential entropy is propagated as described previously. Each component is monitored independently for deviations in the nonlinear and linear predictions of the entropy. Once nonlinearity is detected on a component, the propagation is halted at time t_s, where $t_k \le t_s \le t_{k+1}$. If $t_s \ne t_{k+1}$, then a splitting step is performed on the component for which nonlinearity was detected.** That is, if nonlinearity was detected in the jth component at time t_s, then the jth component is replaced at time t_s by

$$\bar{w}_j p_g(\boldsymbol{x}; \bar{\boldsymbol{\mu}}_j, \bar{\boldsymbol{P}}_j) \approx \sum_{r=1}^{G} w_r p_g(\boldsymbol{x}; \boldsymbol{\mu}_r, \boldsymbol{P}_r)$$

where t_s has been omitted for brevity, and the replacement component weights, means, and covariances are computed using the Gaussian splitting algorithm discussed in [17]. After the splitting step has been performed, return to Eq. (7) with $t_k = t_s$ and $\tilde{N} \leftarrow \tilde{N} + G - 1$ components in the Gaussian mixture, and then continue until $t_s = t_{k+1}$ is reached. Once $t_s = t_{k+1}$, the propagation step has been completed with $\tilde{N}$ components having weights $\tilde{w}_i$, means $\tilde{\boldsymbol{\mu}}_i$, and covariances $\tilde{\boldsymbol{P}}_i$, which allows the propagated conventional GM PDF to be evaluated via Eq. (6).

**Without loss of generality, nonlinearity is assumed to be detected on only one component. If more components detect nonlinearity, the same process is applied to each component individually.

B. AEGIS-Based Approximation of FISST

The AEGIS-FISST approach relies on the fact that, if the (conventional) prior PDF for each object is a GM, then the posterior multiobject (FISST-based) PDF can be approximated by a product of GMs, from which one can extract the (conventional) posterior GM PDFs for each object under the hypothesis that an object exists. This is what distinguishes the proposed method from the GM-PHD approach [8]. The PHD filter approximates the multiobject posterior PDF by its first-order moment, called the intensity function. After that, a GM is used to approximate the intensity function, which gives the GM-PHD approach. The approach proposed in the current work circumvents the first step of approximating the multiobject PDF by its intensity function. Thus, one does not need to approximate the multiobject PDF by its intensity function; instead, one can directly approximate the multiobject PDF using sums of Gaussians.

IV. General Bayesian Multiobject Multiclutter Filter with a Known Number of Objects

A. Prior Density Function

If the number of objects n is known, then the prior multiobject PDF is given by the multi-Bernoulli process [8]

$$f_{k|k}(X|Z^{(k)}) = \sum_{\sigma} f_{k|k}^{\sigma(1)}(\boldsymbol{x}_1|Z^{(k)}) \cdots f_{k|k}^{\sigma(n)}(\boldsymbol{x}_n|Z^{(k)}) \tag{8}$$

for the case where $|X| = n$, with $X = \{\boldsymbol{x}_1, \ldots, \boldsymbol{x}_n\}$ and $Z^{(k)} = \{Z_1, \ldots, Z_k\}$, is the set of all measurement data up to and including step k. The summation in Eq. (8) is taken over all permutations σ of the numbers $1, \ldots, n$. For instance, in the case that $n = 2$, σ may be {1,2} or {2,1}. In the case that $n = 3$, there are six possibilities for σ: {1,2,3}, {1,3,2}, {2,1,3}, {2,3,1}, {3,1,2}, or {3,2,1}. Therefore, for $n = 2$ and $n = 3$, there would be two and six elements to the summation in Eq. (8), respectively. Additionally, $f_{k|k}^{\sigma(i)}(\boldsymbol{x}_i|Z^{(k)})$ in Eq. (8) is the (conventional) PDF for object $\sigma(i)$. It is worth noting that there are n such PDFs, since $\sigma(i) \in \{1, \ldots, n\}$. It is also important to note that, for $|X| \ne n$ $f_{k|k}(X|Z^{(k)}) = 0$ that is, since the number of objects is taken to be known, there is no probability of there being a case where the number of objects is not n. Finally, it is noted that Eq. (8) assumes independence between the objects. This assumption is commonly made in multiobject filters, such as the probability hypothesis density [9] and the cardinalized probability hypothesis density [20] filters, in order to arrive at computationally tractable realizations of the filter.

B. Markov Transitional Density Function

The multiobject motion model without object birth or death is given by

$$f_{k+1|k}(X|X') = \sum_{\sigma} f_{k+1|k}(\boldsymbol{x}_1|\boldsymbol{x}'_{\sigma(1)}) \cdots f_{k+1|k}(\boldsymbol{x}_n|\boldsymbol{x}'_{\sigma(n)}) \tag{9}$$

where $f_{k+1|k}(\boldsymbol{x}_i|\boldsymbol{x}'_i)$, $i = 1, \ldots, n$, is the (conventional) Markov PDF for an object transitioning from state $\boldsymbol{x}'_i$ to state $\boldsymbol{x}_i$. No indexing is needed for the individual Markov PDFs, $f(\boldsymbol{x}_i|\boldsymbol{x}'_i)$, as it is assumed that all objects are subject to the same dynamics. This can be easily generalized for the case when the objects are subject to different dynamics.

C. Multiobject Predicted Density Function

Using the expressions for the prior and Markov transitional density functions given by Eqs. (8) and (9), respectively, and substituting them into the Bayesian predictor of Eq. (1), the propagated PDF is obtained as

$$f_{k+1|k}(X|Z^{(k)}) = \int f_{k+1|k}(X|X')f_{k|k}(X'|Z^{(k)})\delta X'$$

Note that, because $f_{k|k}(X|Z^{(k)}) = 0 \quad \forall\, |X| \neq n$ the set integral definition given in Eq. (4) reduces to a single integral over the continuous states when the set cardinality is n. Therefore, the propagated PDF may be written as

$$f_{k+1|k}(X|Z^{(k)}) = \frac{1}{n!}\int\left(\sum_{\sigma} f_{k+1|k}(\boldsymbol{x}_1|\boldsymbol{x}'_{\sigma(1)})\ \cdots\ f_{k+1|k}(\boldsymbol{x}_n|\boldsymbol{x}'_{\sigma(n)})\right) \times\left(\sum_{\hat{\sigma}} f_{k|k}^{\hat{\sigma}(1)}(\boldsymbol{x}'_1|Z^{(k)})\ \cdots\ f_{k|k}^{\hat{\sigma}(n)}(\boldsymbol{x}'_n|Z^{(k)})\right)\mathrm{d}\boldsymbol{x}'_1\ \cdots\ \mathrm{d}\boldsymbol{x}'_n \tag{10}$$

Carrying out the multiplication in the multiobject predicted density function, it follows that

$$f_{k+1|k}(X|Z^{(k)}) = \sum_{\sigma} f_{k+1|k}^{\sigma(1)}(\boldsymbol{x}_1|Z^{(k)})\ \cdots\ f_{k+1|k}^{\sigma(n)}(\boldsymbol{x}_n|Z^{(k)}) \tag{11}$$

for the case where $|X| = n$. In the preceding equation, $f_{k+1|k}^{\sigma(i)}(\boldsymbol{x}_i|Z^{(k)})$ is the conventional propagated density of object $\sigma(i)$, given that its prior is given by $f_{k|k}^{\sigma(i)}(\boldsymbol{x}'_i|Z^{(k)})$ and its transitional density is given by $f_{k+1|k}(\boldsymbol{x}_i|\boldsymbol{x}'_i)$. The last equality follows from the fact that, when the product within the integrand of Eq. (10) is expanded, $n!$ copies of each of the permuted terms on the right-hand side appear. Hence, the $n!$ terms cancel. Alternatively, Eq. (11) can be written as

$$f_{k+1|k}(X|Z^{(k)}) = \sum_{\sigma}\prod_{i=1}^{n} f_{k+1|k}^{\sigma(i)}(\boldsymbol{x}_i|Z^{(k)}) \tag{12}$$

which is the form that will be used in following developments.

D. Multiobject Measurement Likelihood Density Function

Sensor returns may stem from false alarms (clutter) or objects. In conventional single-object tracking, the measurement likelihood, $f_{k+1}(\boldsymbol{z}|\boldsymbol{x})$, describes the likelihood of getting the measurement $\boldsymbol{z}$ given that the state is $\boldsymbol{x}$. Additionally, objects may not be detected given the state of the object. Therefore, a state-dependent probability of detection, denoted by $p_D(\boldsymbol{x})$, is included. Furthermore, the probability of misdetecting (not detecting) an object with state $\boldsymbol{x}$ is given by $(1 - p_D(\boldsymbol{x}))$. Inclusion of false alarms necessarily dictates that clutter be modeled as well. For this purpose, let clutter be modeled by a Poisson distribution in time with expected value λ and in space with some density function $c(\boldsymbol{z})$. Allowing for misdetections and false alarms, the multiobject likelihood density function is given by [8]

$$f_{k+1}(\varnothing|X) = e^{-\lambda}\prod_{\boldsymbol{x}\in X}(1 - p_D(\boldsymbol{x})) \tag{13}$$

for the case where no measurements are returned and

$$f_{k+1}(Z|X) = e^{\lambda} f_C(Z) f_{k+1}(\varnothing|X)\sum_{\theta}\prod_{i:\ \theta(i)>0}\frac{p_D(\boldsymbol{x}_i)f_{k+1}(\boldsymbol{z}_{\theta(i)}|\boldsymbol{x}_i)}{(1 - p_D(\boldsymbol{x}_i))\lambda c(\boldsymbol{z}_{\theta(i)})} \tag{14}$$

for the case where $m > 0$ measurements are returned [8]. In Eq. (14),

$$f_C(Z) = e^{-\lambda}\prod_{\boldsymbol{z}\in Z}\lambda c(\boldsymbol{z})$$

is the likelihood that Z was generated by clutter. For a detailed discussion on the development of Eqs. (13) and (14), see [8].

The summation in Eq. (14) is taken over all association hypotheses θ: $\{1, \ldots, n\} \to \{0, 1, \ldots, m\}$. With misdetection and false alarm, the number of sensor returns is $m = n - n' + m'$, where n' is the number of misdetections and m' is the number of returns triggered by false alarms. The association function θ takes an input of the object number, $i \in \{1, \ldots, n\}$, and returns a measurement association $\theta(i) \in \{0, 1, \ldots, m\}$. If $\theta(i) > 0$, then the observation $\boldsymbol{z}_{\theta(i)}$ is uniquely associated with the ith object; if $\theta(i) = 0$, then no observation is associated with the ith object (i.e., misdetection of object i). The association function also satisfies the property that for arbitrary i and i'; $\theta(i) = \theta(i') > 0$ implies that $i = i'$ (uniqueness of association). The reader is encouraged to consult [8] for a more in-depth discussion of the association function θ.

E. Bayes Factor

In general, the Bayes factor is given by Eq. (3). Depending on the number of sensor returns, the expression for the Bayes factor can be specifically determined for the given number of returns. The cases considered are 1) no returns, i.e., $Z_{k+1} = \varnothing$; and 2) m returns, i.e., $Z_{k+1} = \{\boldsymbol{z}_1, \ldots, \boldsymbol{z}_m\}$.

For the case of no returns, the multiobject measurement is the empty set $Z_{k+1} = \varnothing$. For the no-return case, the definition of the Bayes factor from Eq. (3) becomes

$$f_{k+1}(Z_{k+1} = \varnothing|Z^{(k)}) = \int f_{k+1}(Z_{k+1} = \varnothing|X)f_{k+1|k}(X|Z^{(k)})\delta X \tag{15}$$

Considering the integrand of Eq. (15), substituting for $f_{k+1|k}(X|Z^{(k)})$ and $f_{k+1}(Z_{k+1}|X)$ from Eqs. (12) and (13), respectively, yields

$$f_{k+1}(Z_{k+1} = \varnothing|X)f_{k+1|k}(X|Z^{(k)}) = \left(e^{-\lambda}\prod_{i=1}^{n}(1 - p_D(\boldsymbol{x}_i))\right)\left(\sum_{\sigma}\prod_{i=1}^{n} f_{k+1|k}^{\sigma(i)}(\boldsymbol{x}_i|Z^{(k)})\right)$$

which may be simplified as

$$f_{k+1}(Z_{k+1} = \varnothing|X)f_{k+1|k}(X|Z^{(k)}) = e^{-\lambda}\sum_{\sigma}\prod_{i=1}^{n}(1 - p_D(\boldsymbol{x}_i))f_{k+1|k}^{\sigma(i)}(\boldsymbol{x}_i|Z^{(k)}) \tag{16}$$

From the definition of a set integral [see Eq. (4)], the Bayes factor is given by

$$f_{k+1}(Z_{k+1} = \varnothing|Z^{(k)}) = \frac{1}{n!}\int f_{k+1}(Z_{k+1}|X)f_{k+1|k}(X|Z^{(k)})\mathrm{d}\boldsymbol{x}_1 \cdots \mathrm{d}\boldsymbol{x}_n$$

which, when Eq. (16) is applied, gives the final form of the Bayes factor in the case of no sensor returns as

$$f_{k+1}(Z_{k+1} = \varnothing|Z^{(k)}) = \frac{e^{-\lambda}}{n!}\sum_{\sigma}\prod_{i=1}^{n}\int(1 - p_D(\boldsymbol{x}_i))f_{k+1|k}^{\sigma(i)}(\boldsymbol{x}_i|Z^{(k)})\mathrm{d}\boldsymbol{x}_i \tag{17}$$

For the case where there is a nonzero number of returns, the multiobject measurement is the m-element set $Z_{k+1} = \{\boldsymbol{z}_1, \ldots, \boldsymbol{z}_m\}$, which has cardinality $m > 0$, i.e., $|Z_{k+1}| = m > 0$. For the case where there are m measurements, the definition of the Bayes factor from Eq. (3) becomes

$$f_{k+1}(Z_{k+1} = \{\boldsymbol{z}_1, \ldots, \boldsymbol{z}_m\}|Z^{(k)}) = \int f_{k+1}(Z_{k+1} = \{\boldsymbol{z}_1, \ldots, \boldsymbol{z}_m\}|X)f_{k+1|k}(X|Z^{(k)})\delta X \tag{18}$$

Considering the integrand of Eq. (18), substituting for $f_{k+1|k}(X|Z^{(k)})$ and $f_{k+1}(Z_{k+1}|X)$ from Eqs. (12) and (14), respectively, yields

$$f_{k+1}(Z_{k+1}=\{z_1,\ldots,z_m\}|X)f_{k+1|k}(X|Z^{(k)})$$
$$=\left(e^{\lambda}f_C(Z_{k+1})f_{k+1}(\varnothing|X)\sum_{\theta}\prod_{i:\,\theta(i)>0}\frac{p_D(\boldsymbol{x}_i)f_{k+1}(z_{\theta(i)}|\boldsymbol{x}_i)}{(1-p_D(\boldsymbol{x}_i))\lambda c(z_{\theta(i)})}\right)$$
$$\times\left(\sum_{\sigma}\prod_{i=1}^{n}f_{k+1|k}^{\sigma(i)}(\boldsymbol{x}_i|Z^{(k)})\right)$$

Using Eq. (13) for $f_{k+1}(\varnothing|X)$, it follows that

$$f_{k+1}(Z_{k+1}=\{z_1,\ldots,z_m\}|X)f_{k+1|k}(X|Z^{(k)})=f_C(Z_{k+1})$$
$$\times\left[\sum_{\theta}\left(\prod_{i:\,\theta(i)>0}\frac{p_D(\boldsymbol{x}_i)}{\lambda c(z_{\theta(i)})}f_{k+1}(z_{\theta(i)}|\boldsymbol{x}_i)\right)\right.$$
$$\left.\times\left(\prod_{i:\,\theta(i)=0}(1-p_D(\boldsymbol{x}_i))\right)\right]\left(\sum_{\sigma}\prod_{i=1}^{n}f_{k+1|k}^{\sigma(i)}(\boldsymbol{x}_i|Z^{(k)})\right)\tag{19}$$

Noting that the product term within the last bracketed term of Eq. (19) may be expressed as

$$\prod_{i=1}^{n}f_{k+1|k}^{\sigma(i)}(\boldsymbol{x}_i|Z^{(k)})=\prod_{i:\,\theta(i)>0}f_{k+1|k}^{\sigma(i)}(\boldsymbol{x}_i|Z^{(k)})\prod_{i:\,\theta(i)=0}f_{k+1|k}^{\sigma(i)}(\boldsymbol{x}_i|Z^{(k)})$$

it is seen that there is a one-to-one correspondence between the product terms within the θ summation and the σ summation of Eq. (19), such that

$$f_{k+1}(Z_{k+1}=\{z_1,\ldots,z_m\}|X)f_{k+1|k}(X|Z^{(k)})=f_C(Z_{k+1})$$
$$\times\sum_{\sigma}\sum_{\theta}\left[\prod_{i:\,\theta(i)>0}\frac{p_D(\boldsymbol{x}_i)}{\lambda c(z_{\theta(i)})}f_{k+1}(z_{\theta(i)}|\boldsymbol{x}_i)f_{k+1|k}^{\sigma(i)}(\boldsymbol{x}_i|Z^{(k)})\right]$$
$$\times\left[\prod_{i:\,\theta(i)=0}(1-p_D(\boldsymbol{x}_i))f_{k+1|k}^{\sigma(i)}(\boldsymbol{x}_i|Z^{(k)})\right]\tag{20}$$

where it is noted that the summations can be interchanged as was done in arriving at Eq. (20). The definition of the set integral is used along with Eqs. (18) and (20) to arrive at the final form of the Bayes factor in the case of m sensor returns as

$$f_{k+1}(Z_{k+1}=\{z_1,\ldots,z_m\}|Z^{(k)})=\frac{f_C(Z_{k+1})}{n!}$$
$$\times\sum_{\sigma}\sum_{\theta}\left[\prod_{i:\,\theta(i)>0}\int\frac{p_D(\boldsymbol{x}_i)}{\lambda c(z_{\theta(i)})}f_{k+1}(z_{\theta(i)}|\boldsymbol{x}_i)f_{k+1|k}^{\sigma(i)}(\boldsymbol{x}_i|Z^{(k)})\,\mathrm{d}\boldsymbol{x}_i\right]$$
$$\times\left[\prod_{i:\,\theta(i)=0}\int(1-p_D(\boldsymbol{x}_i))f_{k+1|k}^{\sigma(i)}(\boldsymbol{x}_i|Z^{(k)})\,\mathrm{d}\boldsymbol{x}_i\right]\tag{21}$$

An easy way to understand the final expression is that, for each possible association hypothesis θ, the states that are associated with a measurement are propagated, detected, and updated (the first set of integral products); the states that are not associated with a measurement are propagated and misdetected (the second set of integral products). The factor outside the summation is to account for all measurements z_i that have not been associated with any state $\boldsymbol{x}_i$.

F. Corrector Step

Bayes' rule for set-valued random variables is given by Eq. (2). As with the Bayes factor, a specific relationship for determining the corrector step is obtained, depending on the number of sensor returns. As such, the cases considered are 1) no returns, i.e. $Z_{k+1}=\varnothing$; and 2) m returns, i.e., $Z_{k+1}=\{z_1,\ldots,z_m\}$.

For $Z_{k+1}=\varnothing$, Bayes' rule yields the corrector step as

$$f_{k+1|k+1}(X|Z_{k+1}=\varnothing,Z^{(k)})=\frac{f_{k+1}(Z_{k+1}=\varnothing|X)f_{k+1|k}(X|Z^{(k)})}{f_{k+1}(Z_{k+1}=\varnothing|Z^{(k)})}\tag{22}$$

The numerator of the right-hand side of Eq. (22) is given by Eq. (16); similarly, the denominator is given by Eq. (17). Therefore, the corrector step for the case of no sensor returns is

$$f_{k+1|k+1}(X|Z_{k+1}=\varnothing,Z^{(k)})$$
$$=\frac{e^{-\lambda}}{f_{k+1}(Z_{k+1}|Z^{(k)})}\sum_{\sigma}\prod_{i=1}^{n}(1-p_D(\boldsymbol{x}_i))f_{k+1|k}^{\sigma(i)}(\boldsymbol{x}_i|Z^{(k)})\tag{23}$$

where $f_{k+1}(Z_{k+1}|Z^{(k)})$ is the Bayes factor for the no-return case, which is given by Eq. (17).

For $|Z_{k+1}|=m>0$, Bayes' rule yields the corrector step as

$$f_{k+1|k+1}(X|Z_{k+1}=\{z_1,\ldots,z_m\},Z^{(k)})$$
$$=\frac{f_{k+1}(Z_{k+1}=\{z_1,\ldots,z_m\}|X)f_{k+1|k}(X|Z^{(k)})}{f_{k+1}(Z_{k+1}=\{z_1,\ldots,z_m\}|Z^{(k)})}\tag{24}$$

The numerator of the right-hand side of Eq. (24) is given by Eq. (20); similarly, the denominator is given by Eq. (21). Therefore, the corrector step for the case of m sensor returns is

$$f_{k+1|k+1}(X|Z_{k+1}=\{z_1,\ldots,z_m\},Z^{(k)})=\frac{f_C(Z_{k+1})}{f_{k+1}(Z_{k+1}|Z^{(k)})}$$
$$\times\sum_{\sigma}\sum_{\theta}\left[\prod_{i:\,\theta(i)>0}\frac{p_D(\boldsymbol{x}_i)}{\lambda c(z_{\theta(i)})}f_{k+1}(z_{\theta(i)}|\boldsymbol{x}_i)f_{k+1|k}^{\sigma(i)}(\boldsymbol{x}_i|Z^{(k)})\right]$$
$$\times\left[\prod_{i:\,\theta(i)=0}(1-p_D(\boldsymbol{x}_i))f_{k+1|k}^{\sigma(i)}(\boldsymbol{x}_i|Z^{(k)})\right]\tag{25}$$

where $f_{k+1}(Z_{k+1}|Z^{(k)})$ is the Bayes factor for the m-return case, which is given by Eq. (21).

V. AEGIS-FISST Filter for Multiobject Multiclutter Filtering

In this section, the FISST equations for the Bayes factor and corrector step computations are developed for the case where the conventional PDFs are represented by Gaussian mixture models. This representation allows for the multiobject PDFs to be completely described by the Gaussian mixture models and for appropriate relationships for the Bayes factor and corrector step to be developed. First, some preliminary definitions of the propagated conventional PDFs and the measurement likelihood are established. Then, the resultant Bayes factor and corrector step equations are developed.

A. Preliminaries

The basic assumption in the AEGIS-FISST algorithm is that the prior, and therefore the propagated (conventional), PDFs can be represented using a weighted sum of Gaussian distributions. Hence, the propagated PDF is given by

$$f_{k+1|k}^{\sigma(i)}(\boldsymbol{x}_i|Z^{(k)})=\sum_{j=1}^{L^{\sigma(i)}}w_j^{\sigma(i)}p_g(\boldsymbol{x}_i;\boldsymbol{m}_j^{\sigma(i)},\boldsymbol{P}_j^{\sigma(i)})\tag{26}$$

where p_g is the Gaussian distribution, $\boldsymbol{m}_j^{\sigma(i)}$ is the jth mean in the Gaussian sum, and $\boldsymbol{P}_j^{\sigma(i)}$ is the jth covariance matrix in the Gaussian sum. Furthermore, $L^{\sigma(i)}$ is the number of components used to approximate the propagated (conventional) PDF belonging to the object $\sigma(i)$. Finally, $w_j^{\sigma(i)}$ is the discrete probability of the jth element within the Gaussian sum representation of the propagated PDF.

The measurement likelihood PDF is also assumed to be Gaussian, such that

$$f_{k+1}(z_{\theta(i)}|\boldsymbol{x}_i) = p_g(z_{\theta(i)}; \boldsymbol{h}(\boldsymbol{x}_i), \boldsymbol{R}) \tag{27}$$

This means that the measurements are assumed to have the form

$$\boldsymbol{z}_{\theta(i)} = \boldsymbol{h}(\boldsymbol{x}_i) + \boldsymbol{v}$$

where $\boldsymbol{h}(\cdot)$ is the nonlinear function that maps the state space into measurement space, and $\boldsymbol{v}$ is the measurement noise. For the measurement likelihood PDF to be taken as Gaussian, it is assumed that the measurement noise is zero mean with covariance $\boldsymbol{R}$. It is worth noting that the assumption of Gaussianity in the measurement likelihood PDF is used for simplicity and ease of exposition. This restriction can be readily lifted in favor of a more general Gaussian mixture model representation [14].

Additionally, a standard identity of products of Gaussian PDFs that is used throughout the derivations is given by

$$p_g(z_{\theta(i)}; \boldsymbol{h}(\boldsymbol{x}_i), \boldsymbol{R}) p_g(\boldsymbol{x}_i; \boldsymbol{m}_j^{\sigma(i)}, \boldsymbol{P}_j^{\sigma(i)}) = q(z_{\theta(i)}) p_g(\boldsymbol{x}_i; \boldsymbol{\mu}_j^{\sigma(i)}, \Sigma_j^{\sigma(i)}) \tag{28}$$

where

$$q(z_{\theta(i)}) = p_g(z_{\theta(i)}; \boldsymbol{y}_j^{\sigma(i)}, \boldsymbol{W}_j^{\sigma(i)}) \tag{29a}$$

$$\boldsymbol{\mu}_j^{\sigma(i)} = \boldsymbol{m}_j^{\sigma(i)} + \boldsymbol{K} \cdot (z_{\theta(i)} - \boldsymbol{y}_j^{\sigma(i)}) \tag{29b}$$

$$\Sigma_j^{\sigma(i)} = \boldsymbol{P}_j^{\sigma(i)} - \boldsymbol{K}\boldsymbol{W}_j^{\sigma(i)}\boldsymbol{K}^T \tag{29c}$$

and

$$\boldsymbol{K} = \boldsymbol{C}_j^{\sigma(i)} \cdot (\boldsymbol{W}_j^{\sigma(i)})^{-1}$$

In Eqs. (29), $\boldsymbol{y}_j^{\sigma(i)}$, $\boldsymbol{W}_j^{\sigma(i)}$, and $\boldsymbol{C}_j^{\sigma(i)}$ are the mean, covariance, and the cross covariance (with the state) of the measurement for the jth component of the $\sigma(i)$th GM PDF, respectively. When the measurement function is nonlinear, linearization can be employed or an unscented transform approach can be used. In the case of the latter, and given a set of K sigma points $\boldsymbol{\chi}_{j,\ell}^{\sigma(i)}$ with associated weights $u_{j,\ell}^{\sigma(i)}$ that represent the mean, $\boldsymbol{m}_j^{\sigma(i)}$ and covariance $\boldsymbol{P}_j^{\sigma(i)}$, a set of measurement transformed sigma points is formed via

$$\mathcal{Z}_{j,\ell}^{\sigma(i)} = h(\boldsymbol{\chi}_{j,\ell}^{\sigma(i)}) \quad \forall\, \ell \in 1, \ldots, K$$

where $\boldsymbol{h}(\cdot)$ is the same nonlinear function that maps the state space into measurement space as before. The mean, covariance, and the cross covariance are then computed as

$$\boldsymbol{y}_j^{\sigma(i)} = \sum_{\ell=1}^{K} u_{j,\ell}^{\sigma(i)} \mathcal{Z}_{j,\ell}^{\sigma(i)}$$

$$\boldsymbol{W}_j^{\sigma(i)} = \sum_{\ell=1}^{K} u_{j,\ell}^{\sigma(i)} (\mathcal{Z}_{j,\ell}^{\sigma(i)} - \boldsymbol{y}_j^{\sigma(i)})(\mathcal{Z}_{j,\ell}^{\sigma(i)} - \boldsymbol{y}_j^{\sigma(i)})^T + \boldsymbol{R}$$

$$\boldsymbol{C}_j^{\sigma(i)} = \sum_{\ell=1}^{K} u_{j,\ell}^{\sigma(i)} (\boldsymbol{\chi}_{j,\ell}^{\sigma(i)} - \boldsymbol{m}_j^{\sigma(i)})(\mathcal{Z}_{j,\ell}^{\sigma(i)} - \boldsymbol{y}_j^{\sigma(i)})^T$$

B. Bayes Factor

1. ∅ Return

Recall that the Bayes factor for no returns is given by Eq. (17). Direct application of the Gaussian mixture representation of the PDF given by Eq. (26) to the Bayes factor of Eq. (17) yields

$$f_{k+1}(Z_{k+1}|Z^{(k)}) = \frac{e^{-\lambda}}{n!} \sum_{\sigma} \prod_{i=1}^{n} \left(1 - \sum_{j=1}^{L^{\sigma(i)}} w_j^{\sigma(i)} \int p_D(\boldsymbol{x}_i) p_g(\boldsymbol{x}_i; \boldsymbol{m}_j^{\sigma(i)}, \boldsymbol{P}_j^{\sigma(i)})\, \mathrm{d}\boldsymbol{x}_i\right)$$

where it is understood that

$$f_{k+1}(Z_{k+1}|Z^{(k)}) = f_{k+1}(Z_{k+1} = \varnothing|Z^{(k)})$$

Noting that the first-order approximation of the integral term is given by the evaluation of $p_D(\boldsymbol{x}_i)$ at the propagated mean $\boldsymbol{m}_j^{\sigma(i)}$, i.e.,

$$\int p_D(\boldsymbol{x}_i) p_g(\boldsymbol{x}_i; \boldsymbol{m}_j^{\sigma(i)}, \boldsymbol{P}_j^{\sigma(i)})\, \mathrm{d}\boldsymbol{x}_i \approx p_D(\boldsymbol{m}_j^{\sigma(i)}) \tag{30}$$

the Bayes factor for the no-return case may be expressed as

$$f_{k+1}(Z_{k+1}|Z^{(k)}) = \frac{e^{-\lambda}}{n!} \sum_{\sigma} \prod_{i=1}^{n} \left(1 - \sum_{j=1}^{L^{\sigma(i)}} w_j^{\sigma(i)} p_D(\boldsymbol{m}_j^{\sigma(i)})\right)$$

which may be rearranged to give the final form of the Bayes factor for the no-return case as

$$f_{k+1}(Z_{k+1} = \varnothing|Z^{(k)}) = \frac{e^{-\lambda}}{n!} \sum_{\sigma} \prod_{i=1}^{n} \left[\sum_{j=1}^{L^{\sigma(i)}} \beta_j^{\sigma(i)}\right] \tag{31}$$

where

$$\beta_j^{\sigma(i)} = (1 - p_D(\boldsymbol{m}_j^{\sigma(i)})) w_j^{\sigma(i)}$$

2. m Returns

Recall that the Bayes factor in this case is given by [see Eq. (21)]

$$f_{k+1}(Z_{k+1}|Z^{(k)}) = \frac{f_C(Z_{k+1})}{n!} \times \sum_{\sigma} \sum_{\theta} \left[\prod_{i:\ \theta(i)>0} \int \frac{p_D(\boldsymbol{x}_i)}{\lambda c(z_{\theta(i)})} f_{k+1}(z_{\theta(i)}|\boldsymbol{x}_i) f_{k+1|k}^{\sigma(i)}(\boldsymbol{x}_i|Z^{(k)})\, \mathrm{d}\boldsymbol{x}_i\right] \times \left[\prod_{i:\ \theta(i)=0} \int (1 - p_D(\boldsymbol{x}_i)) f_{k+1|k}^{\sigma(i)}(\boldsymbol{x}_i|Z^{(k)})\, \mathrm{d}\boldsymbol{x}_i\right] \tag{32}$$

where it is understood that

$$f_{k+1}(Z_{k+1}|Z^{(k)}) = f_{k+1}(Z_{k+1} = \{z_1, \ldots, z_m\}|Z^{(k)})$$

Now, the two bracketed terms in Eq. (32) are considered independently. The form of the propagated given in Eq. (26) and the measurement likelihood PDF in Eq. (27) are applied to the first bracketed term in Eq. (32), yielding

$$\prod_{i:\ \theta(i)>0} \frac{1}{\lambda c(z_{\theta(i)})} \int p_D(\boldsymbol{x}_i) f_{k+1}(z_{\theta(i)}|\boldsymbol{x}_i) f_{k+1|k}^{\sigma(i)}(\boldsymbol{x}_i|Z^{(k)})\, \mathrm{d}\boldsymbol{x}_i = \prod_{i:\ \theta(i)>0} \frac{1}{\lambda c(z_{\theta(i)})} \sum_{j=1}^{L^{\sigma(i)}} w_j^{\sigma(i)} \times \int p_D(\boldsymbol{x}_i) p_g(z_{\theta(i)}; \boldsymbol{h}(\boldsymbol{x}_i), \boldsymbol{R}) p_g(\boldsymbol{x}_i; \boldsymbol{m}_j^{\sigma(i)}, \boldsymbol{P}_j^{\sigma(i)})\, \mathrm{d}\boldsymbol{x}_i \tag{33}$$

Using the Gaussian product identity of Eq. (28), Eq. (33) may be written as

$$\prod_{i:\,\theta(i)>0}\frac{1}{\lambda c(z_{\theta(i)})}\int p_D(\boldsymbol{x}_i)f_{k+1}(z_{\theta(i)}|\boldsymbol{x}_i)f_{k+1|k}^{\sigma(i)}(\boldsymbol{x}_i|Z^{(k)})\,\mathrm{d}\boldsymbol{x}_i$$
$$=\prod_{i:\,\theta(i)>0}\frac{1}{\lambda c(z_{\theta(i)})}\sum_{j=1}^{L^{\sigma(i)}}w_j^{\sigma(i)}q(z_{\theta(i)})\int p_D(\boldsymbol{x}_i)p_g(\boldsymbol{x}_i;\boldsymbol{\mu}_j^{\sigma(i)},\Sigma_j^{\sigma(i)})\,\mathrm{d}\boldsymbol{x}_i \tag{34}$$

where the terms $q(z_{\theta(i)})$, $\boldsymbol{\mu}_j^{\sigma(i)}$, and $\Sigma_j^{\sigma(i)}$ are defined in Eqs. (29). Noting that the first-order approximation of the integral term in Eq. (34) is given by the evaluation of $p_D(\boldsymbol{x}_i)$ at the updated mean $\boldsymbol{\mu}_j^{\sigma(i)}$, i.e.,

$$\int p_D(\boldsymbol{x}_i)p_g(\boldsymbol{x}_i;\boldsymbol{\mu}_j^{\sigma(i)},\Sigma_j^{\sigma(i)})\,\mathrm{d}\boldsymbol{x}_i = p_D(\boldsymbol{\mu}_j^{\sigma(i)})$$

Eq. (34) is given by

$$\prod_{i:\,\theta(i)>0}\frac{1}{\lambda c(z_{\theta(i)})}\int p_D(\boldsymbol{x}_i)f_{k+1}(z_{\theta(i)}|\boldsymbol{x}_i)f_{k+1|k}^{\sigma(i)}(\boldsymbol{x}_i|Z^{(k)})\,\mathrm{d}\boldsymbol{x}_i$$
$$=\prod_{i:\,\theta(i)>0}\frac{1}{\lambda c(z_{\theta(i)})}\sum_{j=1}^{L^{\sigma(i)}}w_j^{\sigma(i)}q(z_{\theta(i)})p_D(\boldsymbol{\mu}_j^{\sigma(i)}) \tag{35}$$

Now, consider the second bracketed term of Eq. (32). The form of the propagated PDF given in Eq. (26) is applied to the second bracketed term in Eq. (32), yielding

$$\prod_{i:\,\theta(i)=0}\left(1-\int p_D(\boldsymbol{x}_i)f_{k+1|k}^{\sigma(i)}(\boldsymbol{x}_i|Z^{(k)})\,\mathrm{d}\boldsymbol{x}_i\right)$$
$$=\prod_{i:\,\theta(i)=0}\left(1-\sum_{j=1}^{L^{\sigma(i)}}w_j^{\sigma(i)}\int p_D(\boldsymbol{x}_i)p_g(\boldsymbol{x}_i;\boldsymbol{m}_j^{\sigma(i)},\boldsymbol{P}_j^{\sigma(i)})\,\mathrm{d}\boldsymbol{x}_i\right)$$

From Eq. (30), it follows that

$$\prod_{i:\,\theta(i)=0}\left(1-\int p_D(\boldsymbol{x}_i)f_{k+1|k}^{\sigma(i)}(\boldsymbol{x}_i|Z^{(k)})\,\mathrm{d}\boldsymbol{x}_i\right)$$
$$=\prod_{i:\,\theta(i)=0}\left(1-\sum_{j=1}^{L^{\sigma(i)}}w_j^{\sigma(i)}p_D(\boldsymbol{m}_j^{\sigma(i)})\right) \tag{36}$$

Substituting Eqs. (35) and (36) into Eq. (32), it follows that the Bayes factor for the m-return case is given by

$$f_{k+1}(Z_{k+1}|Z^{(k)})=\frac{f_C(Z_{k+1})}{n!}$$
$$\times\sum_\sigma\sum_\theta\left[\prod_{i:\,\theta(i)>0}\sum_{j=1}^{L^{\sigma(i)}}\alpha_j^{\sigma(i)}\right]\left[\prod_{i:\,\theta(i)=0}\sum_{j=1}^{L^{\sigma(i)}}\beta_j^{\sigma(i)}\right] \tag{37}$$

where

$$\alpha_j^{\sigma(i)}=\frac{p_D(\boldsymbol{\mu}_j^{\sigma(i)})q(z_{\theta(i)})}{\lambda c(z_{\theta(i)})}w_j^{\sigma(i)}$$
$$\beta_j^{\sigma(i)}=(1-p_D(\boldsymbol{m}_j^{\sigma(i)}))w_j^{\sigma(i)}$$

C. Corrector Step

1. ∅ Return

For the case of no sensor returns, the corrector step was developed in Eq. (23) and, for convenience, it is repeated here as

$$f_{k+1|k+1}(X_{k+1}|Z_{k+1},Z^{(k)})$$
$$=\frac{e^{-\lambda}}{f_{k+1}(Z_{k+1}|Z^{(k)})}\sum_\sigma\prod_{i=1}^{n}((1-p_D(\boldsymbol{x}_i))f_{k+1|k}^{\sigma(i)}(\boldsymbol{x}_i|Z^{(k)}))$$

where it is understood that

$$f_{k+1}(Z_{k+1}|Z^{(k)})=f_{k+1}(Z_{k+1}=\varnothing|Z^{(k)})$$

Applying the form of the propagated conventional PDF given by Eq. (26), and rearranging terms, it follows that the corrector step may be expressed as

$$f_{k+1|k+1}(X_{k+1}|Z_{k+1},Z^{(k)})$$
$$=\frac{e^{-\lambda}}{f_{k+1}(Z_{k+1}|Z^{(k)})}\sum_\sigma\prod_{i=1}^{n}\left[\sum_{j=1}^{L^{\sigma(i)}}w_j^{\sigma(i)}(1-p_D(\boldsymbol{x}_i))p_g(\boldsymbol{x}_i;\boldsymbol{m}_j^{\sigma(i)},\boldsymbol{P}_j^{\sigma(i)})\right]$$

To ensure consistency with the developed relationship for the Bayes factor, $p_D(\boldsymbol{x}_i)$ is evaluated at the propagated mean $\boldsymbol{m}_j^{\sigma(i)}$, yielding the corrector step for the no-return case as

$$f_{k+1|k+1}(X_{k+1}|Z_{k+1},Z^{(k)})$$
$$=\frac{e^{-\lambda}}{f_{k+1}(Z_{k+1}|Z^{(k)})}\sum_\sigma\prod_{i=1}^{n}\left[\sum_{j=1}^{L^{\sigma(i)}}\beta_j^{\sigma(i)}p_g(\boldsymbol{x}_i;\boldsymbol{m}_j^{\sigma(i)},\boldsymbol{P}_j^{\sigma(i)})\right] \tag{38}$$

where it is reminded that

$$\beta_j^{\sigma(i)}=(1-p_D(\boldsymbol{m}_j^{\sigma(i)}))w_j^{\sigma(i)}$$

2. m Returns

In the case that there are m returns, the corrector step takes the form [see Eq. (25)]

$$f_{k+1|k+1}(X_{k+1}|Z_{k+1},Z^{(k)})=\frac{f_C(Z_{k+1})}{f_{k+1}(Z_{k+1}|Z^{(k)})}$$
$$\times\sum_\sigma\sum_\theta\left[\prod_{i:\,\theta(i)>0}\frac{p_D(\boldsymbol{x}_i)}{\lambda c(z_{\theta(i)})}f_{k+1}(z_{\theta(i)}|\boldsymbol{x}_i)f_{k+1|k}^{\sigma(i)}(\boldsymbol{x}_i|Z^{(k)})\right] \tag{39}$$
$$\times\left[\prod_{i:\,\theta(i)=0}(1-p_D(\boldsymbol{x}_i))f_{k+1|k}^{\sigma(i)}(\boldsymbol{x}_i|Z^{(k)})\right]$$

where it is understood that

$$f_{k+1}(Z_{k+1}|Z^{(k)})=f_{k+1}(Z_{k+1}=\{z_1,\ldots,z_m\}|Z^{(k)})$$

The form of the propagated conventional PDF given in Eq. (26) and the measurement likelihood PDF in Eq. (27) are applied in Eq. (39), yielding

$$f_{k+1|k+1}(X_{k+1}|Z_{k+1},Z^{(k)})=\frac{f_C(Z_{k+1})}{f_{k+1}(Z_{k+1}|Z^{(k)})}$$
$$\times\sum_\sigma\sum_\theta\left[\prod_{i:\,\theta(i)>0}\sum_{j=1}^{L^{\sigma(i)}}\frac{p_D(\boldsymbol{x}_i)}{\lambda c(z_{\theta(i)})}w_j^{\sigma(i)}p_g(z_{\theta(i)};\boldsymbol{h}(\boldsymbol{x}_i),\boldsymbol{R})p_g(\boldsymbol{x}_i;\boldsymbol{m}_j^{\sigma(i)},\boldsymbol{P}_j^{\sigma(i)})\right]$$
$$\times\left[\prod_{i:\,\theta(i)=0}\sum_{j=1}^{L^{\sigma(i)}}(1-p_D(\boldsymbol{x}_i))w_j^{\sigma(i)}p_g(\boldsymbol{x}_i;\boldsymbol{m}_j^{\sigma(i)},\boldsymbol{P}_j^{\sigma(i)})\right] \tag{40}$$

Using the Gaussian product identity of Eq. (28) within the first bracketed term of Eq. (40) allows the m-return corrector step to be written as

$$f_{k+1|k+1}(X_{k+1}|Z_{k+1}, Z^{(k)}) = \frac{f_C(Z_{k+1})}{f_{k+1}(Z_{k+1}|Z^{(k)})} \times \sum_{\sigma} \sum_{\theta} \left[\prod_{i:\ \theta(i)>0} \sum_{j=1}^{L^{\sigma(i)}} \frac{p_D(\boldsymbol{x}_i) q(\boldsymbol{z}_{\theta(i)})}{\lambda c(\boldsymbol{z}_{\theta(i)})} w_j^{\sigma(i)} p_g(\boldsymbol{x}_i; \boldsymbol{\mu}_j^{\sigma(i)}, \Sigma_j^{\sigma(i)}) \right] \times \left[\prod_{i:\ \theta(i)=0} \sum_{j=1}^{L^{\sigma(i)}} (1 - p_D(\boldsymbol{x}_i)) w_j^{\sigma(i)} p_g(\boldsymbol{x}_i; \boldsymbol{m}_j^{\sigma(i)}, \boldsymbol{P}_j^{\sigma(i)}) \right] \tag{41}$$

where the terms $q(\boldsymbol{z}_{\theta(i)})$, $\boldsymbol{\mu}_j^{\sigma(i)}$, and $\Sigma_j^{\sigma(i)}$ are defined in Eqs. (29). As before, to ensure consistency with the developed relationship for the Bayes factor in the case of m returns, $p_D(\boldsymbol{x}_i)$ is evaluated at $\boldsymbol{\mu}_j^{\sigma(i)}$ in the first bracketed term of Eq. (41) and at $\boldsymbol{m}_j^{\sigma(i)}$ in the second bracketed term of Eq. (41). After rearranging terms, it follows that the corrector step for m sensor returns is given by

$$f_{k+1|k+1}(X_{k+1}|Z_{k+1}, Z^{(k)}) = \frac{f_C(Z_{k+1})}{f_{k+1}(Z_{k+1}|Z^{(k)})} \times \sum_{\sigma} \sum_{\theta} \left[\prod_{i:\ \theta(i)>0} \sum_{j=1}^{L^{\sigma(i)}} \alpha_j^{\sigma(i)} p_g(\boldsymbol{x}_i; \boldsymbol{\mu}_j^{\sigma(i)}, \Sigma_j^{\sigma(i)}) \right] \times \left[\prod_{i:\ \theta(i)=0} \sum_{j=1}^{L^{\sigma(i)}} \beta_j^{\sigma(i)} p_g(\boldsymbol{x}_i; \boldsymbol{m}_j^{\sigma(i)}, \boldsymbol{P}_j^{\sigma(i)}) \right] \tag{42}$$

where

$$\alpha_j^{\sigma(i)} = \frac{p_D(\boldsymbol{\mu}_j^{\sigma(i)}) q(\boldsymbol{z}_{\theta(i)})}{\lambda c(\boldsymbol{z}_{\theta(i)})} w_j^{\sigma(i)}$$

$$\beta_j^{\sigma(i)} = (1 - p_D(\boldsymbol{m}_j^{\sigma(i)})) w_j^{\sigma(i)}$$

D. Summary

To summarize the AEGIS-FISST method, the multiobject PDF at time t_k is

$$f_{k|k}(X|Z^{(k)}) = \sum_{\sigma} \prod_{i=1}^{n} f_{k|k}^{\sigma(i)}(\boldsymbol{x}_i|Z^{(k)})$$

The propagation of the multiobject PDF yields

$$f_{k+1|k}(X|Z^{(k)}) = \sum_{\sigma} \prod_{i=1}^{n} f_{k+1|k}^{\sigma(i)}(\boldsymbol{x}_i|Z^{(k)})$$

at time t_{k+1} for the case where $|X| = n$ and

$$f_{k+1|k}(X|Z^{(k)}) = 0$$

otherwise. The propagation of each of the conventional PDFs, i.e.,

$$f_{k|k}^{\sigma(i)}(\boldsymbol{x}_i|Z^{(k)}) \rightarrow f_{k+1|k}^{\sigma(i)}(\boldsymbol{x}_i|Z^{(k)})$$

is handled by the use of the AEGIS algorithm [12] n times (one for each conventional PDF).

When a sensor is providing data, either zero or $m > 0$ measurements are received. If zero measurements are recorded, the propagated PDF is updated using Eq. (38) in conjunction with Eq. (31). For the case where $m > 0$ measurements are received, the propagated PDF is updated using Eq. (42) in conjunction with Eq. (37). For each case, the Bayes factor normalizes each of the conventional PDFs such that they integrate, individually, to one, and simultaneously normalize the multiobject PDF, such that the set integral of the posterior multiobject PDF evaluates to one.

To form the posterior Gaussian mixture PDF, the possible σ permutations are first enumerated. For instance, in the case that $n = 2$, the possible permutations are $\sigma = \{1, 2\}$ and $\sigma = \{2, 1\}$, as discussed in Sec. IV.A. Given a σ permutation, the set of association hypotheses θ is determined based on Section IV.D. For each of these pairings, the update of Eq. (38) or Eq. (42) can be constructed, noting that the update for Eq. (38) does not require the association hypotheses. The individual posteriors constructed for each σ, θ pairing are then combined together for all of the association hypotheses independently for each element within σ. All that remains is to combine the updates for the σ permutations. This is done by stacking the updates for the ith object, keeping track of which object is located in which element of the single σ permutation. For the $n = 2$ case, this means that the first set of θ updates from $\sigma = \{1, 2\}$ are combined with the second set of θ updates from $\sigma = \{2, 1\}$.

For cases where more than a few objects are tracked, the number of σ permutations that must be considered becomes computationally infeasible. For instance, when $n = 7$, there are already 5040 permutations to consider. In this case, a prefiltering step is employed to consider only objects capable of generating the data observed. That is, for each object tracked, the conventional measurement likelihood is computed, and only those objects that support a nonzero likelihood of measurement generation are used in forming the σ permutations of the corrector step. All other objects have a zero probability of measurement generation, and are therefore not updated.

The posterior Gaussian sums may exhibit a large increase in the number of components due to updates being performed by data that may or may not actually belong to any given object. For this reason, it is necessary to perform some type of reduction through pruning and merging. In particular, any components with a posterior weight of zero are removed from further consideration, as these components have zero probability of occurring. Second, any components that are identical to one another are blended together, by replacing the collection of the identical components with the same mean and covariance and summing their weights together. This step is necessary, as the association hypotheses contain many combinations of associating the same data to the same object (other elements in the total hypothesis will differ). Finally, and as the only approximation step in the pruning and merging steps, any components that have a weight below a set threshold are removed and the conventional PDF is renormalized to ensure that it remains a valid PDF.

VI. Estimation

Up to this point, the propagation and filtering steps have been derived and discussed in detail but the process of extracting state estimates for each object from the generalized FISST-based PDFs has not been discussed. In other words, given the multiobject posterior PDF

$$f_{k+1|k+1}(X|Z^{(k)})$$

that is obtained from either Eq. (38) or Eq. (42) in AEGIS-FISST, the estimation step seeks to determine an estimate of each of the n objects' states, $\hat{\boldsymbol{x}}_i$, $i \in \{1, \ldots, n\}$. For single-object approaches, the estimate may be defined as the conditional mean of the single-object PDF or as the maximum likelihood (the highest peak) of the single-object PDF. For the case of multiobject PDFs, the joint multitarget (JOM) state estimation [8] approach is employed. The JOM is both Bayes optimal and convergent (statistically consistent), and it is given by

$$\{\hat{\boldsymbol{x}}_1, \ldots, \hat{\boldsymbol{x}}_{\hat{n}}\} = \underset{n, \boldsymbol{x}_1, \ldots, \boldsymbol{x}_n}{\arg\sup} f_{k+1|k+1}(\{\boldsymbol{x}_1, \ldots, \boldsymbol{x}_n\}) \cdot C^n$$

for some constant C. Under the assumption of a fixed, known number of objects n (which is the assumption in this paper), the JOM may be stated as

$$\{\hat{\boldsymbol{x}}_1, \ldots, \hat{\boldsymbol{x}}_n\} = \arg\sup_{\boldsymbol{x}_1,\ldots,\boldsymbol{x}_n} f_{k+1|k+1}(\{\boldsymbol{x}_1, \ldots, \boldsymbol{x}_n\}) \tag{43}$$

i.e., the number of objects is not a parameter of the JOM. From the basic relationship between the set and vector notations [8], and assuming independence between the objects, it follows that

$$\begin{aligned} f_{k+1|k+1}(\{\boldsymbol{x}_1, \ldots, \boldsymbol{x}_n\}) &= n!\sum_{\sigma} f_{k+1|k+1}(\boldsymbol{x}_{\sigma(1)}, \ldots, \boldsymbol{x}_{\sigma(n)}) \\ &= n!\sum_{\sigma}\prod_{i=1}^{n} f^{\sigma(i)}_{k+1|k+1}(\boldsymbol{x}_i) \end{aligned}$$

where the second equality comes from the independence between the objects, and the summation over σ represents the lack of a known track labeling. If a specific labeling is assumed, i.e., $\sigma(i) = i$ $\forall\ i \in \{1, \ldots, n\}$, then

$$f_{k+1|k+1}(\{\boldsymbol{x}_1, \ldots, \boldsymbol{x}_n\}) = n!f(\boldsymbol{x}_1, \ldots, \boldsymbol{x}_n) = n!\prod_{i=1}^{n} f^{(i)}_{k+1|k+1}(\boldsymbol{x}_i) \tag{44}$$

Substituting Eq. (44) into Eq. (43) yields the JOM to be

$$\{\hat{\boldsymbol{x}}_1, \ldots, \hat{\boldsymbol{x}}_n\} = \arg\sup_{\boldsymbol{x}_1,\ldots,\boldsymbol{x}_n} \prod_{i=1}^{n} f^{(i)}_{k+1|k+1}(\boldsymbol{x}_i)$$

where the $n!$ term in Eq. (44) may be neglected due to the assumption of a known number of objects. Due to the independence of the objects, the JOM is equivalent to

$$\hat{\boldsymbol{x}}_i = \arg\sup_{\boldsymbol{x}_i} f^{(i)}_{k+1|k+1}(\boldsymbol{x}_i) \quad \forall\ i \in \{1, \ldots, n\} \tag{45}$$

The estimates $\hat{\boldsymbol{x}}_i$ may then be readily obtained by finding the maximum values of each of the conventional PDFs, $f^{(i)}(\boldsymbol{x}_i)$, which is readily accomplished via an unconstrained optimization problem. Since a specific σ has been assumed, the estimates obtained via Eq. (45) may be mislabeled; the correct σ ordering is determined via examination of the estimation error and assessing which of the σ permutations of $\{\boldsymbol{x}_1, \ldots, \boldsymbol{x}_n\}$ yields the smallest error.

Beyond having the estimates available, it is also desired to be able to compute tracking errors between the AEGIS-FISST solution and the truth. For single-object tracking, this process is straightforward, as there is only one truth and one estimate. That is, the error can readily be defined as the distance between the true and estimates states by using the vector two-norm

$$d(\boldsymbol{x}, \hat{\boldsymbol{x}}) = \|\boldsymbol{x} - \hat{\boldsymbol{x}}\|_2 \tag{46}$$

For multiobject tracking, however, there are two sets that need to be compared: a set of true object states and a set of estimated object states. The sets may be of different cardinality and are not guaranteed to be ordered in a consistent fashion. Therefore, given two arbitrary finite subsets $X = \{\boldsymbol{x}_1, \ldots, \boldsymbol{x}_m\}$ and $\hat{X} = \{\hat{\boldsymbol{x}}_1, \ldots, \hat{\boldsymbol{x}}_n\}$, where $m, n \in \{0, 1, 2, \ldots\}$, the goal is to define a metric to assess how far $\hat{X}$ is from X. To achieve this goal, the optimal subpattern assignment (OSPA) metric [21]

$$\bar{d}^{(c)}_p(X, \hat{X}) = \left[\frac{1}{n}\left(\min_{\pi\in\Pi_n}\sum_{i=1}^{m} d^{(c)}(\boldsymbol{x}_i, \hat{\boldsymbol{x}}_{\pi(i)})^p + c^p(n-m)\right)\right]^{1/p} \tag{47}$$

was introduced as a metric between the two arbitrary sets, where $d^{(c)}(\boldsymbol{x}_i, \hat{\boldsymbol{x}}_{\pi(i)})$ is an arbitrary single-object metric between $\boldsymbol{x}_i$ and $\hat{\boldsymbol{x}}_{\pi(i)}$, and Π_k is the set of permutations on $\{1, 2, \ldots, k\}$ for any $k \in \{1, 2, \ldots\}$. For practical computations, $d^{(c)}(\boldsymbol{x}_i, \hat{\boldsymbol{x}}_{\pi(i)})$ is taken as a cutoff distance defined as

$$d^{(c)}(\boldsymbol{x}_i, \hat{\boldsymbol{x}}_{\pi(i)}) = \min(c, d(\boldsymbol{x}_i, \hat{\boldsymbol{x}}_{\pi(i)}))$$

for $c > 0$, and where $d(\boldsymbol{x}_i, \hat{\boldsymbol{x}}_{\pi(i)})$ is a standard distance metric, such as the vector two-norm given in Eq. (46). For more details on the OSPA metric, including a proof that Eq. (47) is indeed a metric, see [21].

Under the assumption of a fixed, known number of objects n (which is the assumption in this paper), the portion of the OSPA metric that penalizes the cardinality mismatch between X and $\hat{X}$ may be discarded from Eq. (47). Furthermore, because there is no cardinality mismatch, the cutoff value c may be formally set to infinity, which makes the cutoff distance equal to the standard distance. Making these two substitutions reduces the OSPA metric to

$$\bar{d}^{(\infty)}_p(X, \hat{X}) = \left[\frac{1}{n}\left(\min_{\pi\in\Pi_n}\sum_{i=1}^{m} d(\boldsymbol{x}_i, \hat{\boldsymbol{x}}_{\pi(i)})^p\right)\right]^{1/p} \tag{48}$$

Assuming that π^* represents the appropriate permutation to render the minimum summation in Eq. (48) and choosing $p = 1$ gives the OSPA metric to be

$$\bar{d}^{(\infty)}_1(X, \hat{X}) = \frac{1}{n}\sum_{i=1}^{n} d(\boldsymbol{x}_i, \hat{\boldsymbol{x}}_{\pi^*(i)}) \tag{49}$$

The choice of $p = 1$ is merely for convenience, as it can be seen that this yields the OSPA metric as the arithmetic average of the standard vector metric. That is, by choosing $d(\cdot, \cdot)$ to be the vector two-norm, the OSPA metric is the average Euclidean distance between the true object states and their corresponding estimates. Of course, it is still necessary to determine this correspondence (i.e., to determine π^*) in order to compute the OSPA metric.

VII. Optical Sensor Model

In this paper, an optical sensor placed on the surface of the Earth is considered. In two dimensions, the inertial coordinates (x_S, y_S), which represent the geocentric inertial position of the sensor, can be calculated as

$$\begin{aligned} x_S &= R_e \cos\theta_S \\ y_S &= R_e \sin\theta_S \end{aligned}$$

where R_e is the radius of the Earth, and θ_S is the hour angle of the station at the observation epoch, which is given by

$$\theta_S = \theta_0 + \omega(t_k - t_0)$$

Here, θ_0 is the sidereal time of Greenwich at the reference epoch t_0; ω is the angular velocity of the Earth, which is taken to be constant; and t_k is the observation epoch. Given the object's inertial position as (x_T, y_T) at time t_k, the inertial angle with respect to the sensor (see Fig. 1 for a schematic definition of the involved quantities) is

$$\theta_T = \tan^{-1}\frac{y_T - y_S}{x_T - x_S}$$

Note that, for simplicity, the x-y coordinate frame is shown centered at the sensor in Fig. 1; in actuality, the frame is taken to be centered at the center of the Earth. The angle of the boresight with respect to the local vertical is denoted by θ_B, such that the angle with respect to the boresight of the object may be computed as

$$\theta_M = \theta_T - \theta_S - \theta_B \tag{50}$$

The boresight angle serves as a control variable, which provides the pointing of the optical sensor with respect to the local vertical. If θ_M is within a specified half-angle of the field of view f from the boresight, then the measurement of the object at time t_k is given by

$$z_k = \theta_M + v_k \tag{51}$$

where v_k is an additive zero-mean white noise with covariance R. This measurement is made with probability p_D [i.e., there is

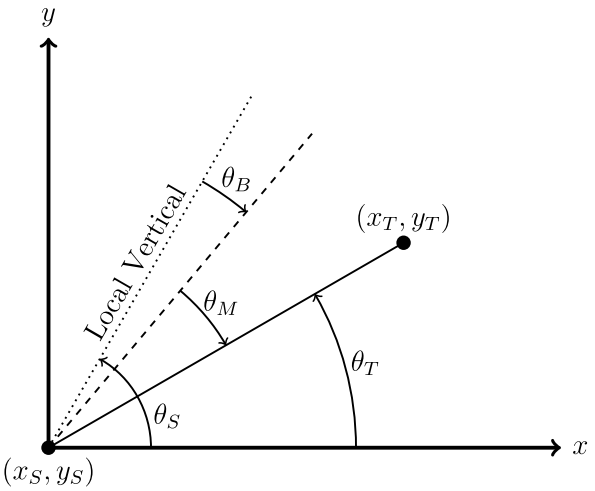

Fig. 1 Schematic depiction of the observation geometry.

probability $(1 - p_D)$ that no measurement is made even when θ_M is within the field-of-view half-angle]. If θ_M is not within the half-angle of the field of view from the boresight, then no return from the object is registered, i.e., $p_D = 0$. The optical measurement model of Eq. (51) is consistent with the formulation of the measurement likelihood PDF of Eq. (27), where $\boldsymbol{h}(\boldsymbol{x}_i)$ is represented by θ_M and described by Eq. (50), and $\boldsymbol{R} = R$ is the measurement noise covariance that represents the statistics of the additive white noise v_k in Eq. (51).

A. Detection Probability

Although not used in this paper, it is worth noting that the probability of detection $p_D(\boldsymbol{x})$ for space object tracking is generally governed by the signal-to-noise ratio (SNR) at the detector. Although the evaluation and modeling of precise SNRs of the probability of detection is beyond the scope of this work, simple geometric considerations can define regions, in which the probability of detection is zero, when either no signal of the object can be received in principle or other light sources overshine the object signal completely.

As already discussed, the first geometric element to the probability of detection is that the object must be within the sensor field of view. If it does not, the probability of detection is zero. Additionally, the observation geometry must be such that the observation time falls within nighttime, starting and ending at civil twilight, and that the object cannot be in close proximity to a line of sight to the moon.

B. False Detection Rate

The contamination by cosmics is here assumed to be the only source of false detections (clutter). The term cosmics subsumes all charged particles impinging the detector during the exposure. Other sources of clutter returns, such as hot or dead pixels, are easily filtered in any astrometric image reduction, so they can safely be neglected here. Observation campaigns with the ESA Space Debris Telescope suggest a maximum number of 30 cosmics per one square degree field of view [22]. This number may be reduced by the use of sensor-specific cosmic filters; classical stacking methods cannot be applied [22,23].

Clutter returns are modeled as a uniform distribution over the field of view; that is, the clutter returns are given by

$$z_k = -f + 2fu$$

where f is the field-of-view half-angle, and u is a random sample from the probability density function $p_u(0, 1)$, which represents a uniform probability density function on [0,1]. Thus, the spatial distribution of clutter is taken to be uniform in this work. The number of clutter returns at any given instant in time is generated by sampling a Poisson distribution with mean parameter λ.

VIII. Simulation Results

To test the proposed approach of AEGIS-FISST for space object tracking, a planar two-body problem is considered for describing the nonlinear dynamical system, i.e., the governing equations of motion for the dynamical system are taken to be

$$\dot{\boldsymbol{r}} = \boldsymbol{v}, \qquad \dot{\boldsymbol{v}} = -\frac{\mu}{r^3}\boldsymbol{r}$$

where $\boldsymbol{r}$ is the inertial position of the object, $\boldsymbol{v}$ is the inertial velocity of the object, $r = \|\boldsymbol{r}\|$, and μ is the gravitational parameter of the Earth. Furthermore, the motion of the vehicle is confined to the equatorial plane, which allows the position to be described by two scalar values, x and y, and the velocity to be described by two scalar values, u and v. Therefore, the state vector and equations of motion that describe the nonlinear dynamical system are

$$\boldsymbol{x}(t) = \begin{bmatrix} x \\ y \\ u \\ v \end{bmatrix} \quad \text{and} \quad \boldsymbol{f}(\boldsymbol{x}(t)) = \begin{bmatrix} u \\ v \\ -\mu x r^{-3} \\ -\mu y r^{-3} \end{bmatrix}$$

where $r = \sqrt{x^2 + y^2}$. To implement the AEGIS approach to propagating uncertainty, the trace of the linearized dynamics Jacobian is also required. This value is readily obtained from the given nonlinear dynamical system as

$$\text{trace}\{\boldsymbol{F}(\boldsymbol{m}(t))\} = \sum_i \frac{\partial f_i(\boldsymbol{x}(t))}{\partial x_i(t)} = 0$$

This then implies that the linearized differential entropy that is used for the detection of nonlinearity within the AEGIS method is constant.

In addition to the nonlinear dynamical system described previously, measurements are generated either from objects in the form

$$\boldsymbol{z}_k = \boldsymbol{h}(\boldsymbol{x}_k) + \boldsymbol{v}_k$$

or from clutter via a uniform distribution over the sensor field of view with the number of clutter returns being a random sample from a Poisson distribution with mean parameter λ, as described in Sec. VII.

Three cases are considered to demonstrate the proposed AEGIS-FISST method: a two-object tracking case with high clutter density, a three-object tracking case with a lower clutter density, and a 25-object tracking case (referred to as the many-object tracking case). In all three cases, the sun is assumed to be in a fixed position with respect to the Earth at a distance of one astronomical unit along the inertial y axis, which determines the times when a station is capable of generating data, i.e., when it is night. For the first two cases, optical measurements (both object-generated and clutter-generated) are simulated on two consecutive nights for 30 min around local midnight (15 min before and 15 minutes after) at a frequency of one measurement per 30 s, with an assumed measurement noise of 2 arcseconds, i.e., the measurement noise covariance is taken to be $R = (2)^2$ arcseconds^2. For the many-object tracking case, the measurements are still simulated on two consecutive nights at a frequency of one measurement per 30 s, with an assumed measurement noise of 2 arcseconds; however, measurements are generated whenever the sun is at least 18 deg below the horizon, which leads to 9.6 h of observation time per night. In all three cases, the probability of detection is $p_D = 0.8$ when the object is within the field of view and zero otherwise. In the two-object tracking case, the mean number of clutter returns is taken to be $\lambda = 10$, and in the three-object and many-object tracking cases, the mean number of clutter returns is taken to be $\lambda = 5$. In all three cases, clutter is generated via a uniform spatial distribution across the sensor field of view, which is taken to have a half-angle of 2 deg.

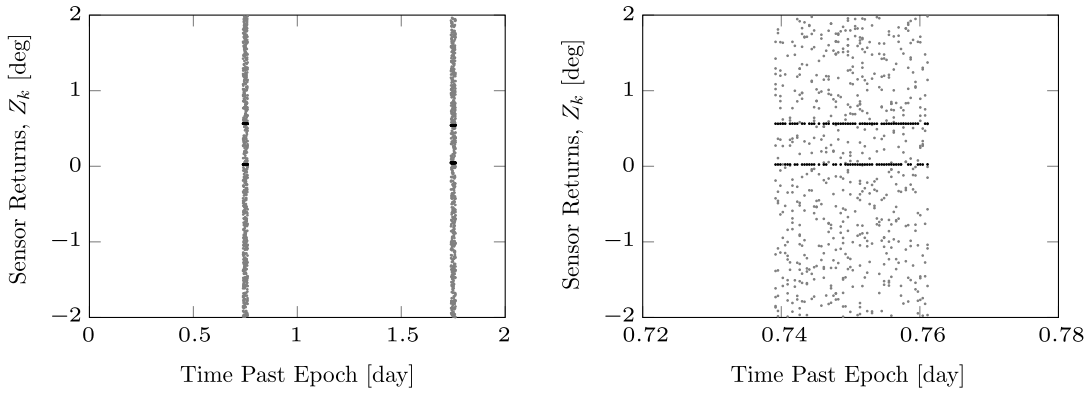

a) Sensor return values **b) Sensor return values (first night only)**

Fig. 2 Values of the sensor returns as a function of time for the two-object tracking case.

A. Results: Two-Object Tracking

The first set of results is obtained tracking two objects in orbit. The first object has an initial mean, which is characterized by the orbital elements of semimajor axis, eccentricity, argument of periapse, and mean anomaly of

$$a = 42164.173 \text{ km}, \qquad e = 0,$$
$$\omega = 0 \text{ deg}, \quad \text{and} \quad M = 0 \text{ deg}$$

Similarly, the second object has an initial mean that is characterized by

$$a = 42164.173 \text{ km}, \qquad e = 0,$$
$$\omega = 0 \text{ deg}, \quad \text{and} \quad M = 0.5 \text{ deg}$$

Both objects are taken to have an initial uncertainty that is Gaussian with a diagonal covariance matrix with standard deviation values of 1 km in position and 0.1 m/s in velocity.

Figure 2 illustrates the sensor returns, both from object-generated and clutter-generated measurements as a function of time, with Fig. 2a showing the measurements for both nights and Fig. 2b focusing on only the measurements generated during the first night. For visualization purposes only, Fig. 2 depicts the returns from clutter in gray and the returns from objects in black; the algorithm has no knowledge of this distinction. The effects of the state-dependent probability of detection are observed in Fig. 2b, wherein the occasional misdetection of an object is evident. Figure 3 shows the number of sensor returns, including both object- and clutter-generated returns, as a function of time. From Fig. 3, it can be seen that there are as many as 21 measurements reported from the sensor. Figures 4a and 4b illustrate the position and velocity tracking error as a function of time, respectively. Figures 5a and 5b give the OSPA metric [computed from Eq. (49)] as a function of time, where Fig. 5b focuses in on the time around which data are generated during the second night.

From Fig. 4, it is seen that the initial uncertainty in the object's states causes both the position and velocity error to increase until the measurements begin on the first night. The processing of the first night's data causes the position and velocity error to diminish. Between the two nights, both the position and velocity errors grow, but at a substantially decreased rate, when compared to the initial error growth. Processing the second night's data again diminishes the position and velocity errors, and it further mitigates subsequent error growth. From Fig. 5, it can be seen that the growth of uncertainty causes the OSPA metric to increase up to the time when data become available during the first night and, at a slower rate, between the two nights. Since the OSPA metric combines both position and velocity errors, and since the position errors are larger in magnitude than the velocity errors, the OSPA metric is dominated by the position errors. Once all of the data have been processed, both objects have position errors less than 500 m and velocity errors smaller than 5 cm/s. Examination of Fig. 5 in fact shows that the OSPA metric after all of the data has been processed is approximately 0.45, indicating that the average position error is approximately 450 m.

B. Results: Three-Object Tracking

In this example, it is assumed that there are three objects in orbit. Returns from clutter are shown in gray, and returns from objects are shown in black. Note that two of the objects are observed very near to one another during the first night. The first two objects have initial means characterized as in the previous example. The third object has an initial mean that is characterized by the orbital elements

$$a = 42,264.173 \text{ km}, \qquad e = 0.01,$$
$$\omega = 0 \text{ deg}, \quad \text{and} \quad M = 2.2 \text{ deg}$$

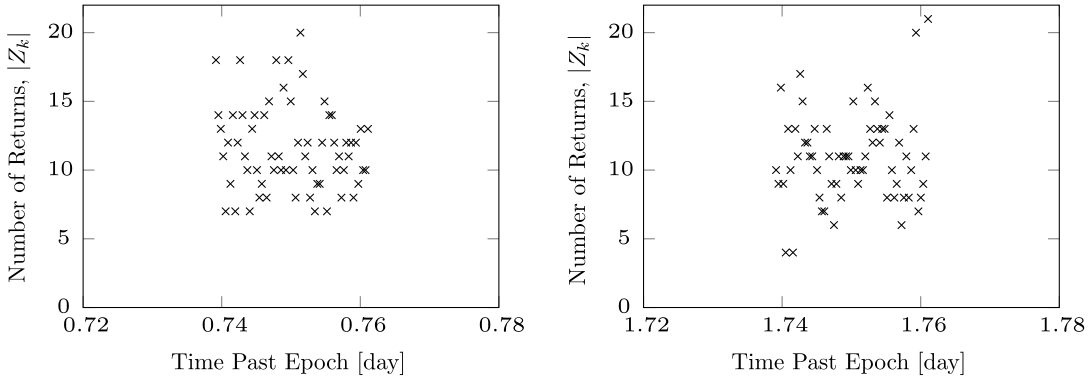

a) Number of sensor returns, first night **b) Number of sensor returns, second night**

Fig. 3 Number of sensor returns as a function of time for the two-object tracking case.

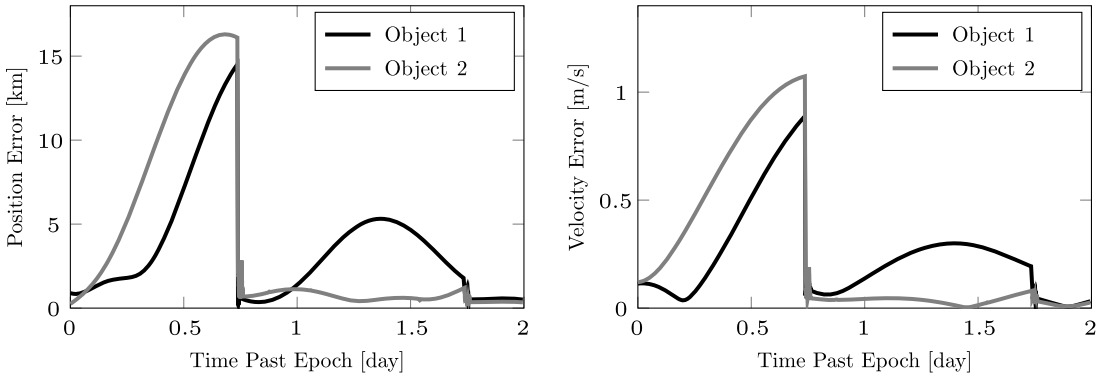

a) Position error **b) Velocity error**

Fig. 4 Position and velocity estimation error as a function of time for the two-object tracking case.

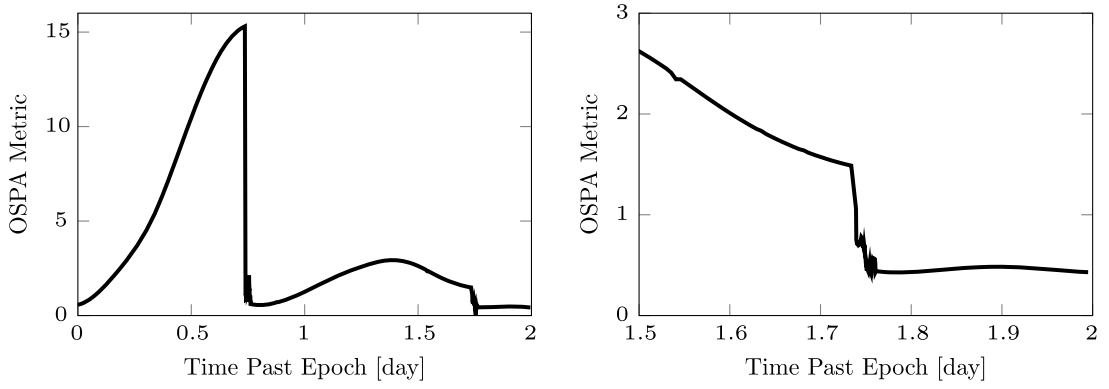

a) Entire run **b) Second night only**

Fig. 5 OSPA metric as a function of time for the two-object tracking case.

All three objects have an initial uncertainty characterized by a Gaussian distribution with diagonal covariance characterized by standard deviation values of 1 km in position and 0.1 m/s in velocity.

Figure 6 illustrates the sensor returns both from object-generated and clutter-generated measurements as a function of time, with Fig. 6a showing the measurements for both nights and Fig. 6b focusing on only the measurements generated during the first night. Figure 7 shows the number of sensor returns, including both object-generated and clutter-generated returns, as a function of time. Figures 8a and 8b illustrate the position and velocity tracking error as a function of time, respectively. Figures 9a and 9b give the OSPA metric [computed from Eq. (49)] as a function of time.

As seen in Fig. 6, there are three objects for which data are simulated. Although Fig. 6 shows the data generated by clutter and by objects separately, AEGIS-FISST has no knowledge which data originated from clutter and which originated from the objects. From Fig. 6, it can be seen that two of the objects are in close proximity to one another during the time when data are collected on the first night and that one object "crosses" the other (from a measurement point of view) in going from the first night to the second night. Figure 7 shows that there are between 2 and 14 sensor returns at any given time, with an approximate average of eight returns throughout the entire simulation (five from clutter and three from objects).

Similar to the two-object tracking example, Fig. 8 shows that the three-object tracking example exhibits an initial error growth until data become available on the first night. Once measurements are available, both the position and velocity errors quickly decrease. Unlike the two-object tracking case, there is a large spike in the position tracking error of object 1 and the velocity tracking error of objects 1 and 3 at the beginning of the first set of data. This error spike

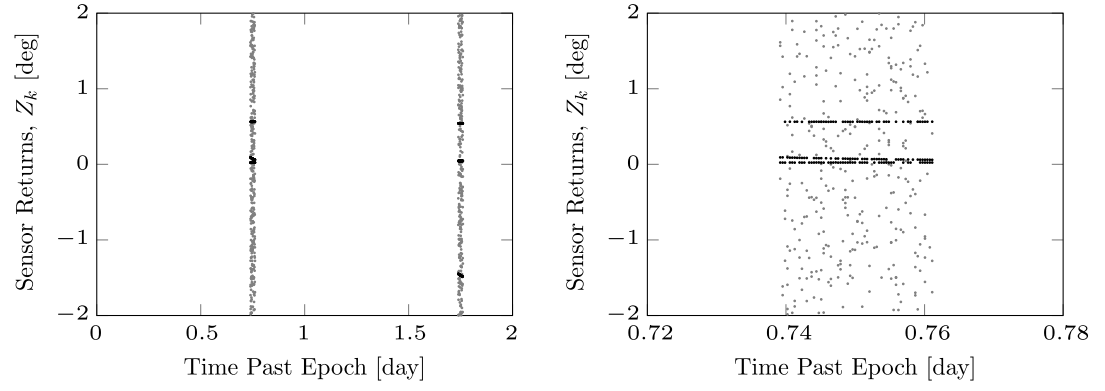

a) Sensor return values **b) Sensor return values (first night only)**

Fig. 6 Values of the sensor returns as a function of time for the three-object tracking case.

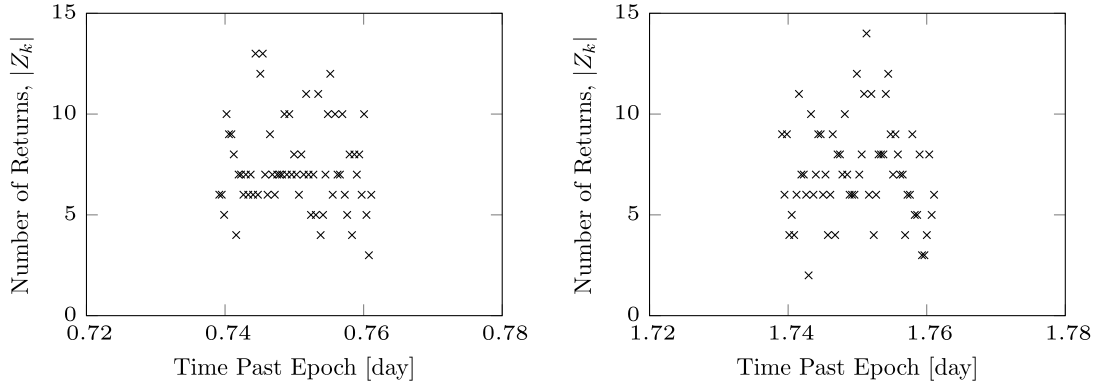

a) Number of sensor returns, first night **b) Number of sensor returns, second night**

Fig. 7 Number of sensor returns as a function of time for the three-object tracking case.

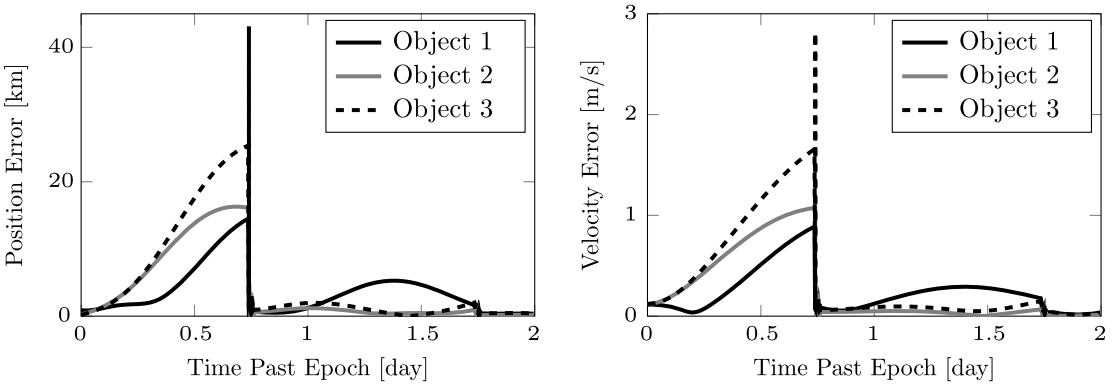

a) Position error **b) Velocity error**

Fig. 8 Position and velocity estimation error as a function of time for the three-object tracking case.

is caused by a confusion between the two closely spaced (in measurement space) objects as well as by a confusion with a clutter return, which happens due to the large uncertainties in the object's conventional PDF. Furthermore, it is observed that the error spike quickly dissipates as more data are made available and the algorithm is able to separate between the data from the closely spaced objects and the data generated by clutter. Processing data from the second night again diminishes the position and velocity errors, and it further mitigates subsequent error growth during periods of no data. Once all of the data have been processed, all three objects have position errors less than 500 m and velocity uncertainties smaller than 5 cm/s. Since the OSPA metric, shown in Fig. 9, is an average of the tracking errors, the spike in error seen in the tracking of object 3 does not show up in the OSPA metric. Examination of Fig. 9b shows that the OSPA metric after the data from the second night is processed is approximately 0.32, indicating that the average position error is approximately 320 m.

C. Results: Many-Object Tracking

For the final example, it is assumed that there are 25 objects in orbit. The objects are randomly generated, such that each one has a semimajor axis of $a_{\text{geo}} - 500 \text{ km} \leq a \leq a_{\text{geo}} + 500 \text{ km}$, with a_{geo} being the semimajor axis of a geosynchronous orbit, with an eccentricity of $0 \leq e \leq 0.2$, a mean anomaly of $-25 \text{ deg} \leq M \leq 25 \text{ deg}$, and an argument of periapse of zero for all objects. All 25 objects have an initial uncertainty characterized by a Gaussian distribution that has a diagonal covariance matrix with standard deviation values of 1 km in position and 0.1 m/s in velocity. The orbits for the many-object tracking case are

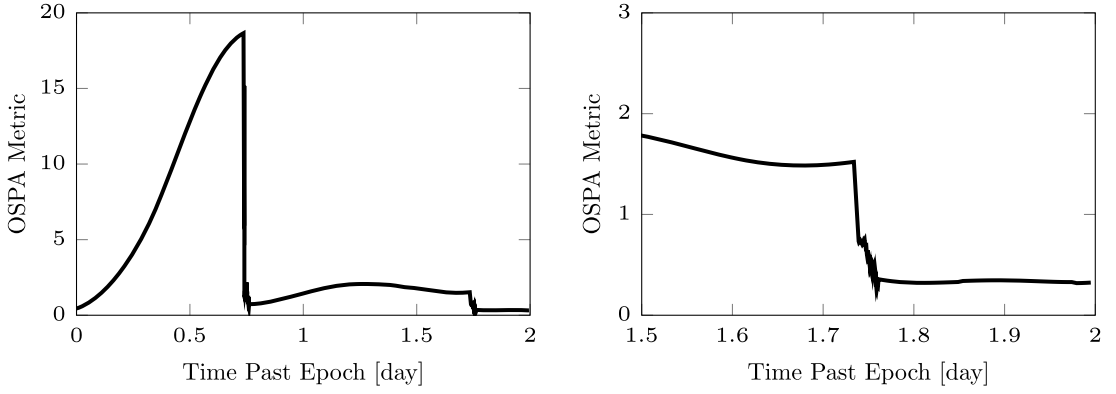

a) Entire run **b) Second night only**

Fig. 9 OSPA metric as a function of time for the three-object tracking case.

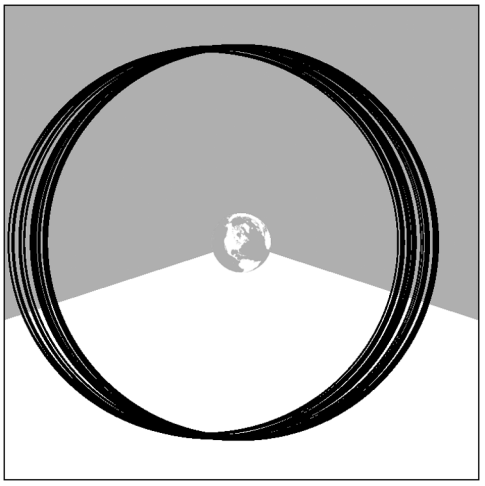

Fig. 10 Schematic representation of the orbits in the many-object tracking case.

shown in Fig. 10. In Fig. 10, the Earth is shown for scale, and the gray region represents the portion of the orbits not observed by the sensor.

In both the two-object and three-object tracking cases, the sensor was fixed with the boresight along the local vertical, i.e., $\theta_B = 0$ in Fig. 1. For the many-object tracking case, the sensor boresight angle is allowed to vary within $\theta_B = \pm 45$ deg so that a larger region may be observed. This is accomplished by scheduling the sensor to sweep through the boresight angle starting at $\theta_B = +45$ deg at the beginning of the night and ending at $\theta_B = -45$ deg at the end of the night. The sweep rate is assumed to be constant throughout the night. As discussed previously, night is taken to be the period of time when the sun is at least 18 deg below the horizon, which leads to 9.6 h of observation time per night. Figure 10 illustrates the region of the orbits where observations are simulated. The gray region denotes the portion of the orbits where observations are not available. The white region is the region directly overhead of the sensor when observations are being simulated. As the boresight moves, any objects that are within a half-angle of 2 deg (i.e., any objects within the moving field of view of the sensor) are detected with a probability of detection of $p_D = 0.8$. Any objects that are outside of the sensor's field of view are not detected; that is, $p_D = 0$ outside of the sensor's field of view.

Figure 11a illustrates the sensor returns, both from object-generated (black) and clutter-generated (gray) measurements, and Fig. 11b shows the number of sensor returns as a function of time. There are between zero and three objects within the field of view at any given time, and there are between 0 and 13 clutter-generated returns at any given time. Figures 12a and 12b illustrate the position tracking error and OSPA metric as a function of time, respectively. Figures 13a and 13b give the position tracking error and OSPA metric as a function of time during the second night.

As opposed to the two-object and three-object tracking cases, where it is relatively easy to see the separate objects within the data, the simulated data in the many-object tracking case are not easily separated into individual objects. The number of objects, as well as the boresight motion of the sensor, renders the individual object tracks indistinguishable in Fig. 11a. For the many-object tracking case, there are between 1 and 15 sensor returns at any given time, as shown in Fig. 11b, which does not significantly change from the three-object tracking case (between 2 and 14 returns). The lack of change between these cases is explained by the motion of the sensor, which limits the number of objects in the field of view but expands the region that can be observed.

Figure 12 shows that, like the previous cases, the many-object tracking example exhibits an initial error growth until the measurements begin on the first night. Once measurements are available, the position errors quickly decrease, as does the OSPA

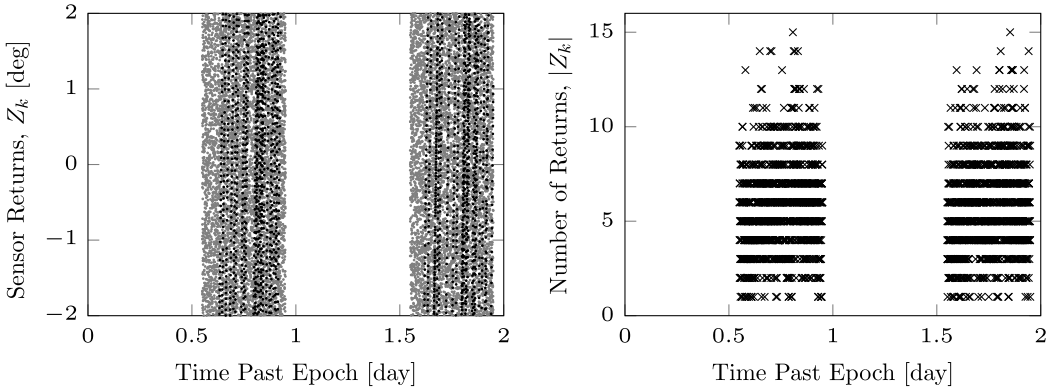

a) Sensor return values **b) Number of sensor returns**

Fig. 11 Values and number of sensor returns as a function of time for the many-object tracking case.

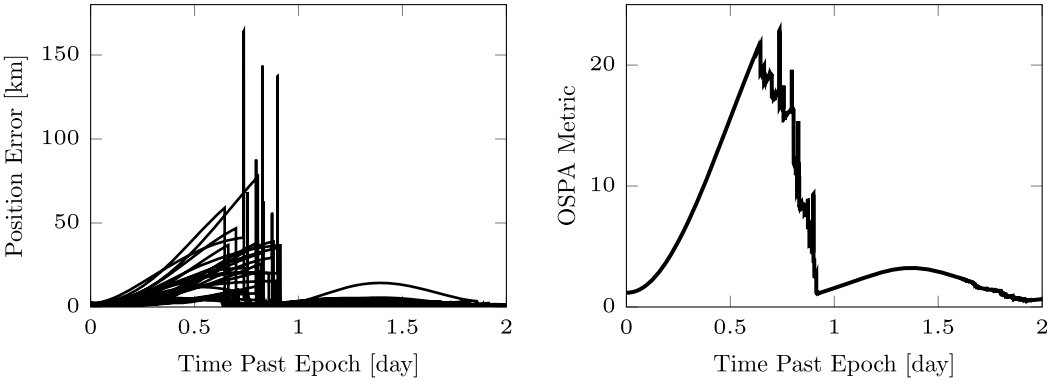

a) Position error **b) OSPA Metric**

Fig. 12 Position estimation error and the OSPA metric as a function of time for the many-object tracking case.

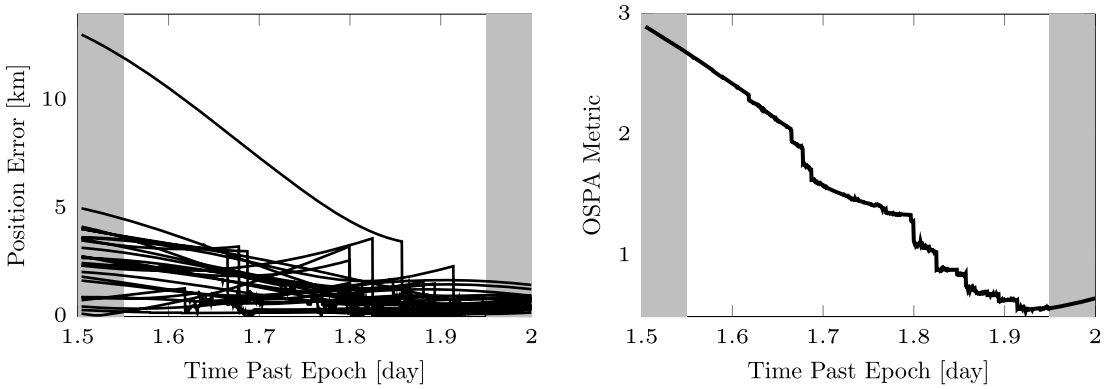

a) Position error b) OSPA Metric

Fig. 13 Position estimation error and the OSPA metric as a function of time for the many-object tracking case during the second night.

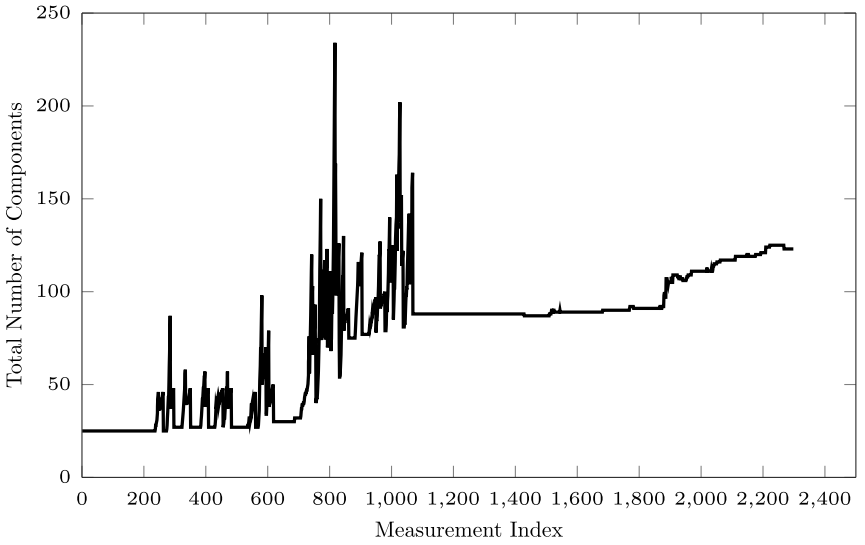

Fig. 14 Number of components in the posterior Gaussian sum (after pruning and merging) as a function of the measurement index.

metric. Similar to the three-object tracking case, there are large spikes in the tracking error of individual objects during the first night. Each spike occurs during the time when the first data are associated to the object, which is why the spikes are distributed throughout the first night. However, each error spike quickly dissipates as more data are made available and the algorithm successfully distinguishes each object from the others as well as from data that are generated by clutter.

The position error and OSPA metric during the second night are highlighted in Fig. 13. The position errors for all objects and the OSPA metric are further reduced due to the inclusion of additional data. The gray-shaded regions in Fig. 13 show the periods where no data are available. Close examination shows that there are periods where data are available but very little change (due to the incorporation of the data) is observed in the position errors or the OSPA metric. This is because there are no object-originated data during this time, which can be seen in Fig. 11a. Examination of Fig. 13b shows that the OSPA metric after all of the data have been processed is approximately 0.57, indicating that the average position error in tracking each of the 25 objects is approximately 570 m.

Additionally, the number of total components in the multiobject PDF is shown in Fig. 14. The total number of components is computed by summing the components in each conventional PDF after the measurement update has occurred and after the pruning and merging steps have been completed. Transient behavior is observed with large increases to the number of components whenever data are first processed. This is due to a combination of the increased object uncertainties that allows multiple object-generated and clutter-generated data to be processed against multiple objects. Although the transients tend to decrease over time, there is still an observed increase in the number of components that remains throughout the data processing. This leaves a final complexity of between four and five components per object. It is possible that more advanced merging algorithms could be used to obviate this trend.

IX. Conclusions

In this paper, finite-set statistics is used to solve the joint data association and tracking problem in the presence of misdetections, false alarms, and noisy data, where false alarms are triggered by a Poisson-distributed clutter model. An adaptive Gaussian mixtures approach is used to solve the multiobject uncertainty propagation problem and serves as the basis for the approximation of the various multiobject finite-set statistics-based probability density functions. This is based on the observation that, if the multiobject prior density is given by an appropriate sum of Gaussians, then the posterior density will also be a sum of Gaussians, under appropriate and reasonable assumptions. This allows for the retention of a higher degree of information content than in first-order approximation methods such as the probability hypothesis density filter.

The proposed finite-set statistics method was applied to several numerical examples for space surveillance tracking, and the tracking error performance was analyzed in each case. It was shown that the proposed method successfully tracked the objects in all cases, with average terminal tracking errors of between 320 and 570 m when provided with line-of-sight data accurate to 2 arcseconds on two consecutive nights. The presence of clutter-originated returns and closely spaced (in the measurement space) objects was shown to

cause temporary performance degradation when the prior solution had a high level of uncertainty. Additionally, the inclusion of additional measurement data from follow-on tracking allowed the proposed method to separate the true target returns from the clutter-generated data in every instance, which enabled the successful tracking and localization of each target.

Acknowledgments

The authors would like to acknowledge the financial support of the U.S. Air Force Office of Scientific Research and the National Research Council. This paper is approved for public release: 377ABW-2014-0581.

References

[1] Schildknecht, T., "Optical Surveys for Space Debris," *Astronomy and Astrophysics Review*, Vol. 14, No. 1, 2007, pp. 41–111. doi:10.1007/s00159-006-0003-9

[2] Kelecy, T., and Jah, M., "Analysis of High Area-to-Mass Ratio (HAMR) GEO Space Object Orbit Determination: Initial Strategies to Recover and Predict HAMR GEO Trajectories with No a Priori Information," *Acta Astronautica*, Vol. 69, Nos. 7–8, 2011, pp. 551–558. doi:10.1016/j.actaastro.2011.04.019

[3] Hall, D., Calef, B., Knox, K., Bolden, M., and Kervin, P., "Separating Attitude and Shape Effects for Non-resolved Objects," *Advanced Maui and Space Surveillance Technologies (AMOS) Conference*, Curran Associates, Red Hook, NY, Sept. 2007.

[4] DeMars, K. J., Jah, M. K., and Schumacher, P. W., "Initial Orbit Determination using Short-Arc Angle and Angle Rate Data," *IEEE Transactions on Aerospace and Electronic Systems*, Vol. 43, No. 3, July 2012, pp. 2628–2637. doi:10.1109/TAES.2012.6237613

[5] Maruskin, J. M., Scheeres, D. J., and Alfriend, K. T., "Correlation of Optical Observations of Objects in Earth Orbit," *Journal of Guidance, Control, and Dynamics*, Vol. 32, No. 1, Jan.–Feb. 2009, pp. 194–209. doi:10.2514/1.36398

[6] Früh, C., Schildknecht, T., Musci, R., and Ploner, M., "Catalogue Correlation of Space Debris Objects," *Proceedings of the Fifth European Conference on Space Debris*, ESA Communication Production Office, Noordwijk, The Netherlands, 2009.

[7] Goodman, I. R., Mahler, R. P. S., and Nguyen, H. T., *Mathematics of Data Fusion*, Kluwer, Dordrecht, The Netherlands, 1997, pp. 131–174, 175–218, Chaps. 4, 5.

[8] Mahler, R. P. S., *Statistical Multisource-Multitarget Information Fusion*, Artec House, Norwood, MA, 2007, pp. 483–537, 655–682, Chaps. 14, 17.

[9] Vo, B., and Ma, W., "The Gaussian Mixture Probability Hypothesis Density Filter," *IEEE Transactions on Signal Processing*, Vol. 54, No. 11, Nov. 2006, pp. 4091–4104. doi:10.1109/TSP.2006.881190

[10] Mahler, R. P. S., "Multitarget Markov Motion Models," *SPIE Conference on Signal Processing, Sensor Fusion, and Target Recognition VIII*, Vol. 3720, July 1999, pp. 47–58. doi:10.1117/12.357192

[11] DeMars, K. J., Bishop, R. H., and Jah, M. K., "A Splitting Gaussian Mixture Method for the Propagation of Uncertainty in Orbital Mechanics," *Proceedings of the AAS/AIAA Space Flight Mechanics Meeting, Vol. 140, Advances in the Astronautical Sciences*, Univelt, San Diego, CA, Feb. 2011, pp. 1419–1438.

[12] DeMars, K. J., Bishop, R. H., and Jah, M. K., "Entropy-Based Approach for Uncertainty Propagation of Nonlinear Dynamical Systems," *Journal of Guidance, Control, and Dynamics*, Vol. 36, No. 4, July–Aug. 2013, pp. 1047–1057. doi:10.2514/1.58987

[13] Hussein, I., DeMars, K. J., Früh, C., Erwin, R. S., and Jah, M. K., "An AEGIS-FISST Integrated Detection and Tracking Approach to Space Situational Awareness," *Proceedings of the 15th International Conference of Information Fusion*, IEEE, Piscataway, NJ, July 2012, pp. 2065–2072.

[14] Sorenson, H. W., and Alspach, D. L., "Recursive Bayesian Estimation Using Gaussian Sums," *Automatica*, Vol. 7, No. 4, Aug. 1971, pp. 465–479. doi:10.1016/0005-1098(71)90097-5

[15] Alspach, D. L., and Sorenson, H. W., "Nonlinear Bayesian Estimation Using Gaussian Sum Approximations," *IEEE Transactions on Automatic Control*, Vol. 17, No. 4, Aug. 1972, pp. 439–448. doi:10.1109/TAC.1972.1100034

[16] Terejanu, G., Singla, P., Singh, T., and Scott, P., "Uncertainty Propagation for Nonlinear Dynamic Systems using Gaussian Mixture Models," *Journal of Guidance, Control, and Dynamics*, Vol. 31, No. 6, Nov.–Dec. 2008, pp. 1623–1633. doi:10.2514/1.36247

[17] DeMars, K. J., "Nonlinear Orbit Uncertainty Prediction and Rectification for Space Situational Awareness," Ph.D. Thesis, Univ. of Texas, Austin, TX, 2010.

[18] Vallée, R, "Information Entropy and State Observation of a Dynamical System," *Uncertainty in Knowledge-Based Systems*, edited by Bouchon, B., and Yager, R., Vol. 286, Lecture Notes in Computer Science, Springer, Berlin, 1987, pp. 403–405. doi:10.1007/3-540-18579-8_38

[19] Julier, S. J., Uhlmann, J. K., and Durrant-Whyte, H. F., "A New Approach for Filtering Nonlinear Systems," *Proceedings of the American Control Conference*, Vol. 3, June 1995, pp. 1628–1632. doi:10.1109/ACC.1995.529783

[20] Vo, B.-T., Vo, B.-N., and Cantoni, A., "Analytic Implementations of the Cardinalized Probability Hypothesis Density Filter," *IEEE Transactions on Signal Processing*, Vol. 55, No. 7, July 2007, pp. 3553–3567. doi:10.1109/TSP.2007.894241

[21] Schuhmacher, D., Vo, B.-T., and Vo, B.-N., "A Consistent Metric for Performance Evaluation of Multi-Object Filters," *IEEE Transactions on Signal Processing*, Vol. 56, No. 8, 2008, pp. 3447–3457. doi:10.1109/TSP.2008.920469

[22] Früh, C., and Schildknecht, T., "Object Image Linking of Objects in Near Earth Orbits in the Presence of Cosmics," *Advances in Space Research*, Vol. 49, No. 3, 2012, pp. 594–602. doi:10.1016/j.asr.2011.10.021

[23] Früh, C., *Identification of Space Debris*, Shaker Verlag, Aachen, Germany, 2011, pp. 31–54, Chap. 5.